TERA

NUREG/CR-0844
ORNL/NUREG/TM-329

LMFBR Aerosol Release and Transport Program Quarterly Progress Report for January-March 1979

T. S. Kress
J. T. Han

Prepared for the U.S. Nuclear Regulatory Commission
Office of Nuclear Regulatory Research
Under Interagency Agreements DOE 40-551-75 and 40-552-75

OAK RIDGE NATIONAL LABORATORY
OPERATED BY UNION CARBIDE CORPORATION · FOR THE DEPARTMENT OF ENERGY

Printed in the United States of America. Available from
National Technical Information Service
U.S. Department of Commerce
5285 Port Royal Road, Springfield, Virginia 22161

NUREG/CR-0844
ORNL/NUREG/TM-329
Dist. Category R7

Contract No. W-7405-eng-26

Engineering Technology Division

LMFBR AEROSOL RELEASE AND TRANSPORT PROGRAM QUARTERLY PROGRESS REPORT FOR JANUARY–MARCH 1979

T. S. Kress J. T. Han

Manuscript Completed – July 9, 1979
Date Published – August 1979

Prepared for the
U.S. Nuclear Regulatory Commission
Office of Nuclear Regulatory Research
Under Interagency Agreements DOE 40-551-75 and 40-552-75

NRC FIN No. B0121

Prepared by the
OAK RIDGE NATIONAL LABORATORY
Oak Ridge, Tennessee 37830
operated by
UNION CARBIDE CORPORATION
for the
DEPARTMENT OF ENERGY

CONTENTS

FOREWORD

This report summarizes progress under the Liquid-Metal Fast Breeder Reactor (LMFBR) Aerosol Release and Transport (ART) Program [sponsored by the Division of Reactor Safety Research of the Nuclear Regulatory Commission (NRC)] for the period January–March 1979.

Work on this program was initially reported as Volume III of a four-volume series entitled *Quarterly Progress Report on Reactor Safety Programs Sponsored by the NRC Division of Reactor Safety Research*. Prior reports of this series are

Report No.	Period covered
ORNL/TM-4655	April–June 1974
ORNL/TM-4729	July–September 1974
ORNL/TM-4805	October–December 1974
ORNL/TM-4914	January–March 1975
ORNL/TM-5021	April–June 1975

Beginning with the report covering the period July–September 1975, work under this program is now being reported as *LMFBR Aerosol Release and Transport Program Quarterly Progress Report*. Prior reports under this title are

Report No.	Period covered
ORNL/NUREG/TM-8	July–September 1975
ORNL/NUREG/TM-9	October–December 1975
ORNL/NUREG/TM-35	January–March 1976
ORNL/NUREG/TM-59	April–June 1976
ORNL/NUREG/TM-75	July–September 1976
ORNL/NUREG/TM-90	October–December 1976
ORNL/NUREG/TM-113	January–March 1977
ORNL/NUREG/TM-142	April–June 1977
ORNL/NUREG/TM-173	July–September 1977
ORNL/NUREG/TM-193	October–December 1977
ORNL/NUREG/TM-213	January–March 1978
ORNL/NUREG/TM-244	April–June 1978
ORNL/NUREG/TM-276	July–September 1978
ORNL/NUREG/TM-318	October–December 1978

Copies of all these reports are available from the Technical Information Center, Oak Ridge, Tennessee 37830.

SUMMARY

J. T. Han

The Aerosol Release and Transport (ART) from Liquid-Metal Fast Breeder Reactor (LMFBR) Fuel Program at Oak Ridge National Laboratory (ORNL) is designed to investigate the release and transport of radionuclides that may result from a hypothetical core-disruptive accident (HCDA) in an LMFBR. The experimental program is being conducted in three facilities: the Fuel Aerosol Simulant Test (FAST)/Containment Research Installation (CRI-III), the Nuclear Safety Pilot Plant (NSPP), and the CRI-II. The analytical effort is designed to support the experiments as well as to provide independent assessment of the consequences of an HCDA.

During this report period, 15 tests were performed in the FAST/CRI-III facility. These consisted of five high-temperature argon tests in the FAST vessel and eight vacuum and two underwater tests in the CRI-III vessel.

In the high-temperature argon tests, the FAST vessel was maintained at a temperature of 866 to 922°K (1100 to 1200°F); aerosol mass concentration and plateout samples were taken. There were no major problems encountered in obtaining the measurements.

The first five "Sandia Normalization" tests were performed in CRI-III at near vacuum pressure. The capacitor discharge vaporization (CDV) energy input was in the range of 18 to 28 kJ; the UO_2 debris produced in the tests were sampled using a rotating wheel collector developed at Sandia to provide droplet size and velocity measurements.

Two underwater tests were performed in CRI-III to evaluate the performance of the high-temperature submersible pressure-measuring equipment. It was found that the transducer cable vibration caused signal noise. This problem seems to have been solved by damping out any possible cable vibrations; however, more underwater tests will be performed to ensure the accuracy of the pressure measurements.

In the NSPP experimental program, the dc plasma torch uranium oxide generator was installed, and two tests were made to evaluate its performance. The aerosol concentrations in the tests performed were much lower than expected, because the powder feed unit of the system became plugged

shortly after powder feed was initiated. This problem apparently was caused by the use of particle sizes that were finer than in previous tests in CRI-II. Tests using larger particle sizes will be performed.

Particle size distributions of uranium oxide aerosols measured with inertial impactors in CRI-II experiments have been compared with simultaneous measurements using a spiral centrifuge. Results indicate that the impactor-measured diameters are significantly smaller than the centrifuge-measured diameters. This disagreement in size measurements appears to have been caused by the fragmentation of the "chain-like" U_3O_8 agglomerates in the impactors. Such a conclusion is also supported by sizes estimated from the concentration decay curves. Calculations are also presented for the average sizes of uranium oxide agglomerates and the number of primary particles per agglomerate.

Additional analytical studies were performed in support of the NSPP test program. First, a fallout model equivalent to that used in the HAARM-3 aerosol code was used to estimate fallout rates to be expected from particle size and aerosol concentration measurements in NSPP tests. The results for Na_2O aerosols were compared with the actual fallout measurements. Second, a simple analytical method was used to estimate the magnitude of the buoyancy-induced air velocity (from the NSPP temperature and pressure measurements) that will sustain a practically well-mixed aerosol system in the NSPP vessel. Third, comparison of a drag coefficient correlation for spherical particles with existing data is shown to be excellent for a wide range of Reynolds numbers.

GLOSSARY OF ACRONYMS

ACRR	Annular Core Research Reactor
AMMD	Aerodynamic Mass Median Diameter
ART	Aerosol Release and Transport
CDA	core-disruptive accident
CDV	capacitor discharge vaporization
CRI	Containment Research Installation
DAS	data acquisition system
FAST	Fuel Aerosol Simulant Test
HCDA	hypothetical core-disruptive accident
LASL	Los Alamos Scientific Laboratory
LMFBR	Liquid-Metal Fast Breeder Reactor
NRC	Nuclear Regulatory Commission
NSPP	Nuclear Safety Pilot Plant
ORNL	Oak Ridge National Laboratory

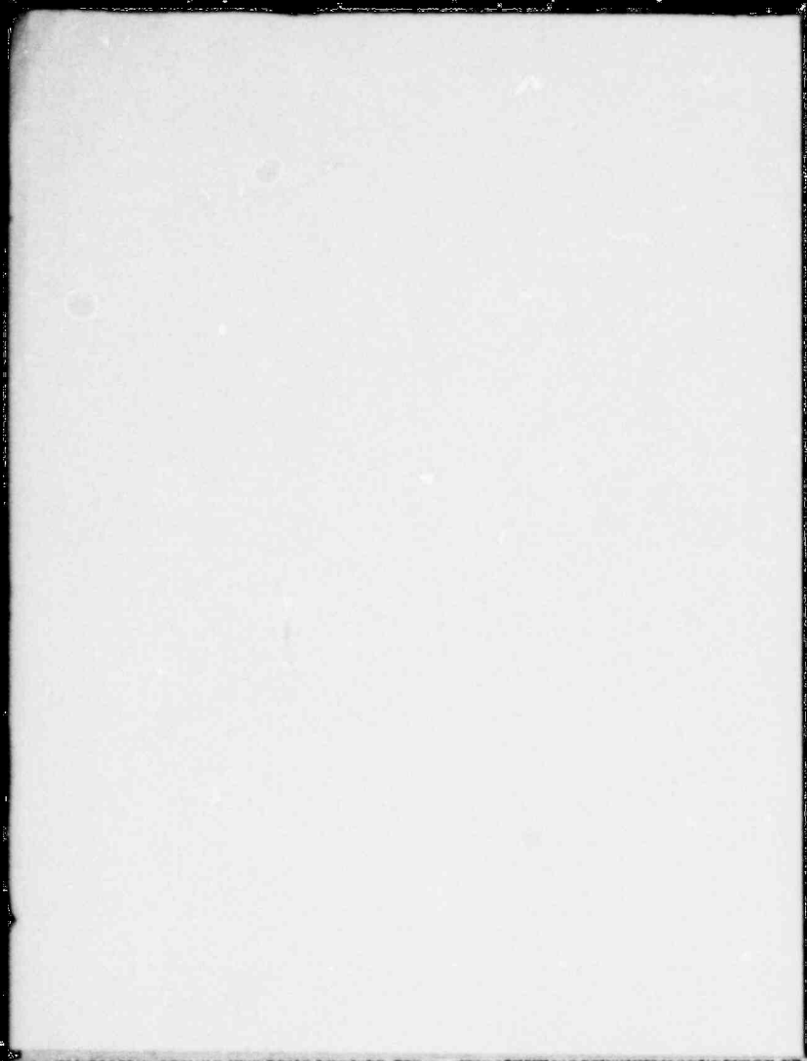

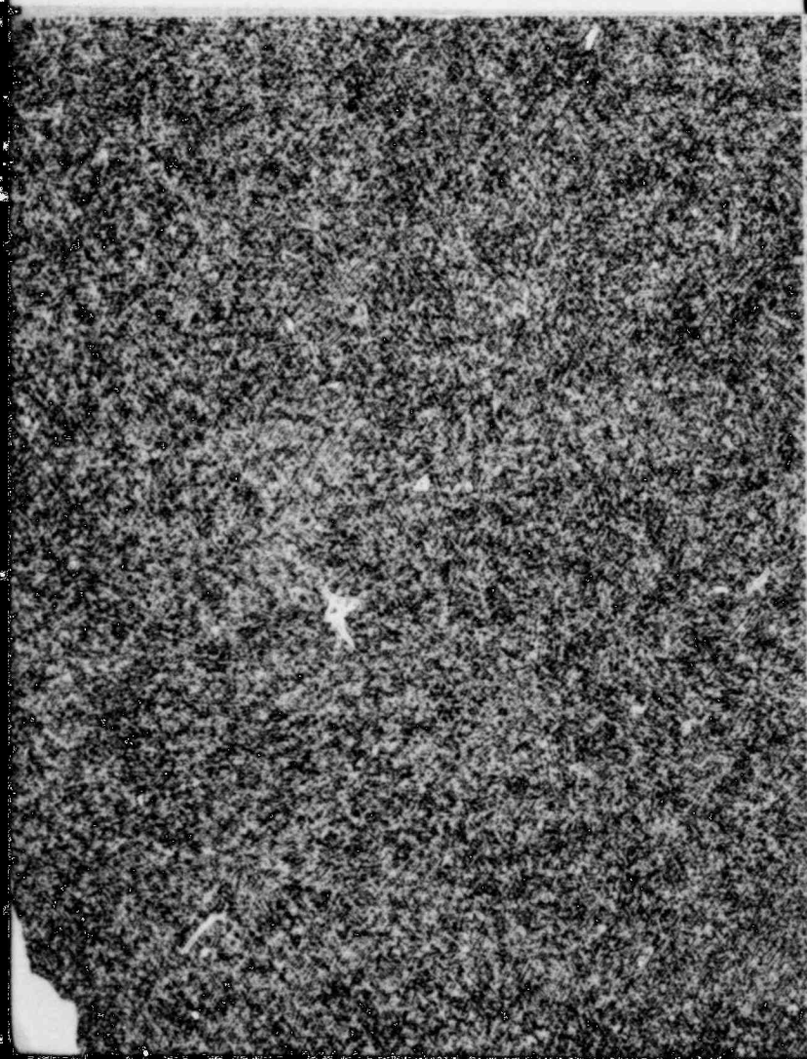

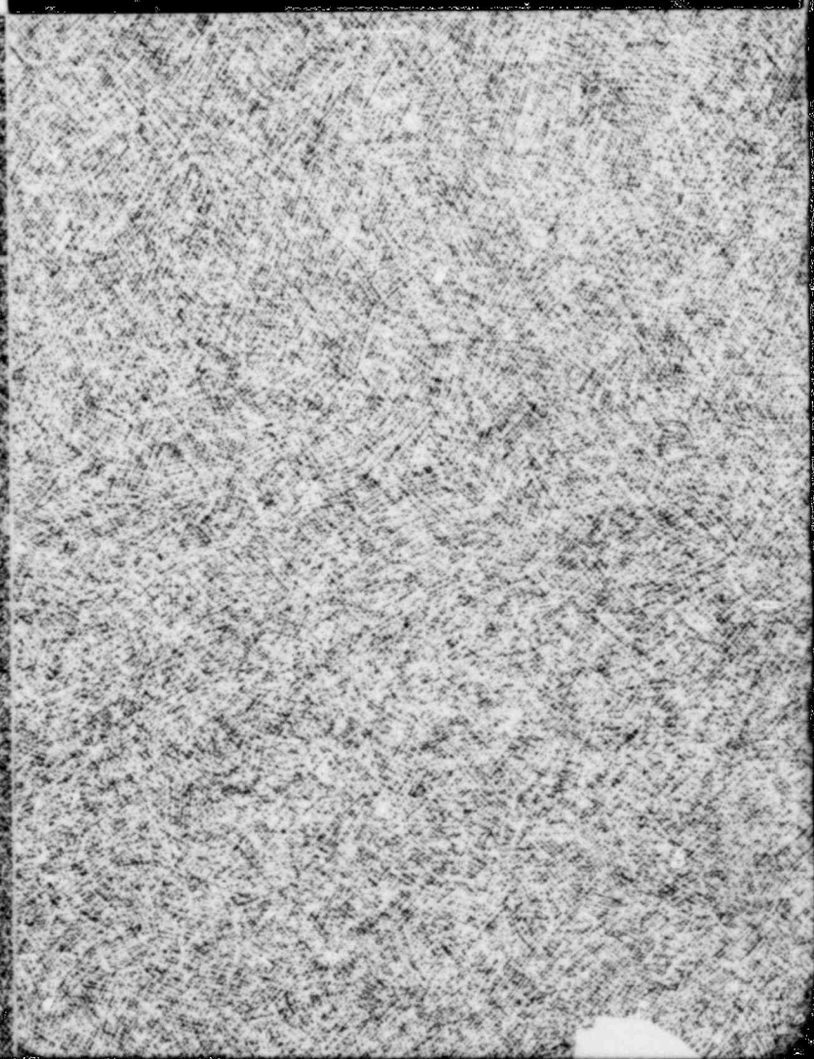

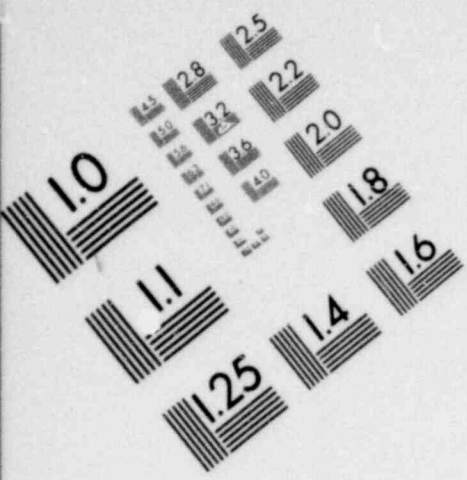

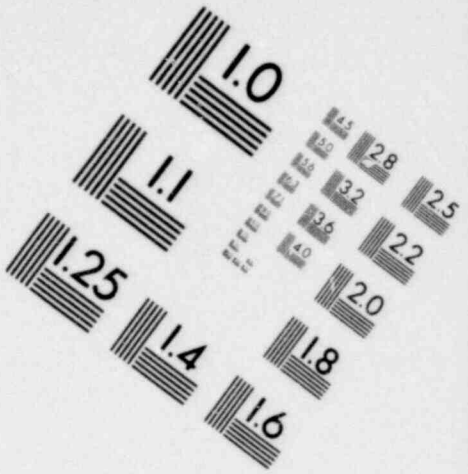

IMAGE EVALUATION TEST TARGET (MT-3)

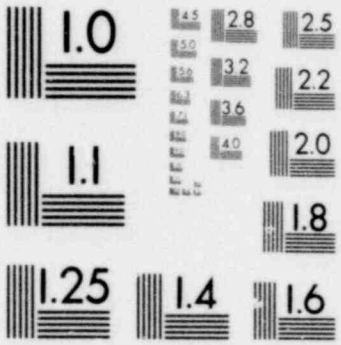

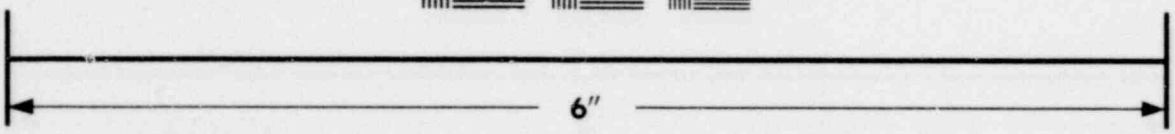

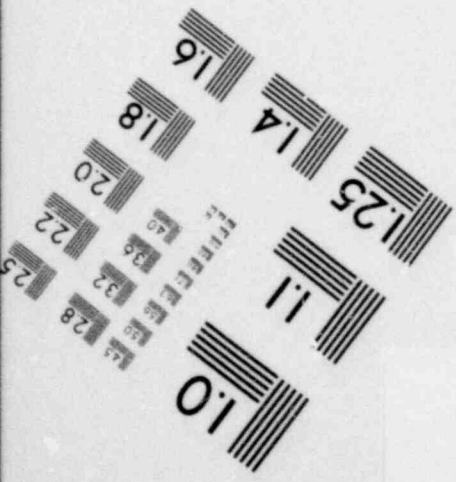

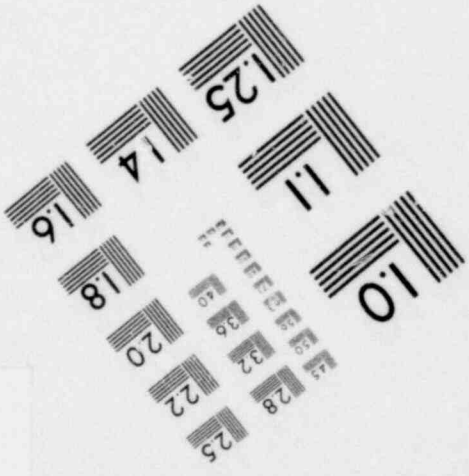

LMFBR AEROSOL RELEASE AND TRANSPORT PROGRAM QUARTERLY PROGRESS REPORT FOR JANUARY–MARCH 1979

T. S. Kress

ABSTRACT

This report summarizes progress for the Liquid-Metal Fast Breeder Reactor (LMFBR) Aerosol Release and Transport (ART) Program sponsored by the Division of Reactor Safety Research of the Nuclear Regulatory Commission (NRC) for the period January–March 1979. This program is designed to investigate radionuclide release and transport from LMFBRs for reactor events of severity up to and including hypothetical core-disruptive accidents (HCDAs). Program topics discussed include recent capacitor discharge vaporization (CDV) tests in the Fuel Aerosol Simulant Test (FAST)/Containment Research Installation (CRI-III) facility, including underwater and vacuum tests in the CRI-III vessel; fuel-oxide tests in the Nuclear Safety Pilot Plant (NSPP) using a newly installed dc plasma metal-oxygen torch; fuel-oxide aerosol size measurements using two different instruments in the CRI-II facility, and calculated results of average size and number of primary particles per aerosol agglomerate; an evaluation of the HAARM-3 code fallout model using NSPP data; and the development of a simple analytical method to estimate the buoyancy-induced air velocity in the NSPP tests.

Keywords: aerosol, hypothetical accident, LMFBR fission product release, fission product transport, ex-reactor experiment, safety, radionuclide transfer, uranium.

1. INTRODUCTION

The Liquid-Metal Fast Breeder Reactor (LMFBR) Aerosol Release and Transport (ART) Program at Oak Ridge National Laboratory (ORNL), sponsored by the Division of Reactor Safety Research of the Nuclear Regulatory Commission (NRC), is an LMFBR safety program concerned with radionuclide release and transport. The scope includes radionuclide release from fuel, transport to and release from primary containment boundaries, and behavior within containments. The overall goal of the program is to provide the analytical methods and experimental data necessary to assess the quantity and transient behavior of radionuclides released from LMFBR cores as a result of postulated events of varying severity up to and including severe hypothetical core-disruptive accidents (HCDAs).

The program is divided into several related experimental and analytical activities as summarized below:

1. development of a capacitor discharge vaporization (CDV) system for deposition of energy in simulated LMFBR fuel (UO_2) that will provide a nonnuclear means for studying the fuel response to HCDA-like energy depositions;
2. development of alternative means for generating fuel-simulant aerosols on a relatively continuous basis;
3. study of the characteristics and behavior of fuel-simulant aerosols in several small vessels, including the effects of radiation and the simultaneous vaporization of small amounts of sodium;
4. production and study of fuel-simulant and sodium aerosols in the Nuclear Safety Pilot Plant (NSPP) for validation of models with particular emphasis on scaling features relative to containment size;
5. study of the fuel interactions, expansion, and thermal behavior within the sodium pool as the resultant fuel vapor bubble is transported through the sodium to the cover-gas region.

Varying levels of effort are anticipated within these categories, with analytical modeling accompanying the experimental work. The analytical requirements fall into four categories: (1) fuel response to high rates of energy deposition, (2) fuel-bubble dynamic behavior and transport characteristics under sodium, (3) dynamic aerosol behavior at high concentrations in the bubble and containment atmospheres, and (4) pretest prediction and posttest comparison of the NSPP experiment using the HAARM-3 code.

An attempt will be made to consolidate the analyses and data and to present them in a manner that will facilitate direct assessment of the radiological hazard associated with arbitrary hypothetical accident scenarios.

2. EXPERIMENTAL PROGRAM

2.1 SIMMER Verification and Source Term Experiments in FAST/CRI-III

A. L. Wright A. M. Smith J. M. Rochelle

2.1.1 Introduction

During this quarter, 15 tests were performed in the Fuel Aerosol Simulant Test (FAST)/Containment Research Installation (CRI-III) facility, including 5 in the FAST vessel and 10 in the CRI-III vessel. These tests were of three types:

1. five high-temperature FAST argon tests (FAST 12 through 16) performed at standard pressure and at argon temperatures greater than 866 K (1100°F);
2. two underwater tests in CRI-III using the FAST vaporizer assembly (CDV 67 and 68);
3. eight vacuum tests in CRI-III — the first three tests (CDV 69 through 71) were in preparation for the "Sandia Normalization" tests, and the final five tests (CDV 72 through 76) were the first five Sandia Normalization tests.

Data for these tests are presented in Tables 1 to 3. Individual test results and conclusions are presented in Sects. 2.1.2 to 2.1.4.

2.1.2 Discussion of results of FAST vaporizer underwater tests in CRI-III

Two underwater tests were performed in CRI-III this quarter. Previous test results[1] have shown that a vapor bubble can be produced in water and that this bubble rapidly condenses (in <100 msec). However, no pressure measurements were attempted in the previous tests, and CDV 67 and 68 were performed to test the operation of the pressure-measuring equipment.

CDV 67. As in most previous water tests, the water height above the test section was 20.3 cm (8 in.) and the argon gas pressure was at ~0.101 MPa (1 atm). A 3000-psia Kaman Sciences pressure transducer (time response <1 msec) was installed ~15.2 cm (6 in.) from the vaporizer. Signal

Table 1. Sample data

Test No.	Pellet stack mass (g)	Pellet stack length (cm)	Microsphere mass (g)	Quartz tube ID–OD (cm)
FAST 12	18.48	8.95	30.94	0.972–1.66
FAST 13	17.38	9.02	30.43	0.970–1.63
FAST 14	17.43	9.06	31.30	0.969–1.69
FAST 15	17.56	9.10	30.60	0.972–1.66
FAST 16A	17.56	9.19	31.91	0.972–1.66
CDV 67	17.64	9.15	32.02	0.970–1.72
CDV 68	17.57	9.12	32.11	0.970–1.72
CDV 69	21.52	11.20	38.98	0.974–1.71
CDV 70A	21.53	11.40	40.00	0.970–1.67
CDV 71	21.41	11.12	40.23	0.970–1.66
CDV 72	21.30	11.09	34.74	*a*–1.65
CDV 73	21.43	11.17	35.06	*a*–1.65
CDV 74	21.67	11.29	34.93	*a*–1.66
CDV 75	21.41	11.14	35.95	*b*–1.67
CDV 76	21.55	11.20	34.60	*c*–1.66

[a] Special tubes used for CDV 72, 73, 74; see Figs. 6 and 7.

[b] Tube has ends bored to 0.975 cm ID, center fire-polished section with 0.922 cm ID.

[c] Special tube used for CDV 76; see Figs. 8 and 9.

Table 2. High preheat and CDV charging data[a]

Test No.	High preheat power (W)	Sample resistance after high preheat (Ω)	Number of capacitor banks charged	Charging voltage (V)	Initial bank energy (kJ)
FAST 12	1600	0.41	4	1945	75
FAST 13	1700	0.38	4	1945	75
FAST 14	1700	0.39	4	1850	68
FAST 15	1500	0.50	4	1950	75
FAST 16A	*b*	*b*	6	2500	180
CDV 67	1800	0.44	4	1950	75
CDV 68	1800	0.44	4	1945	75
CDV 69	2200	0.48	4	1945	75
CDV 70A	2200	0.49	4	1845	68
CDV 71	2200	0.49	4	1945	75
CDV 72	2200	0.52	4	1950	75
CDV 73	2200	0.52	4	1945	75
CDV 74	2200	0.55	4	1945	75
CDV 75	2200	0.48	4	1950	75
CDV 76	2200	0.48	4	1950	75

[a] High preheat lasts for 28 sec; there is a 2-sec delay between high preheat and capacitor discharge.

[b] No preheat in FAST 16A test.

Table 3. Energy input and aerosol yield data

Test No.	CDV time to arcing (msec)	CDV energy deposited before arcing (kJ)	Estimated initial aerosol yield ($\mu g/cm^3$)	Estimated initial aerosol mass (g)[a]
FAST 12[b]	1.57	18.3	2.72	1.24
FAST 13[b]	1.85	22.5	2.60	1.18
FAST 14[b]	2.01	21.7	2.83	1.29
FAST 15[b]	2.73	29.0	3.41	1.55
FAST 16A[b]	0	0	0	0
CDV 67	1.75	~21.8[c]	0	0
CDV 68	3.50	~44.7[c]	0	0
CDV 69	2.40	25.4	*d*	*d*
CDV 70A	9.25[e]	57.4[e]	*d*	*d*
CDV 71	7.36	59.5	*d*	*d*
CDV 72	2.02	18.3	*d*	*d*
CDV 73	0.22	1.4	*d*	*d*
CDV 74	2.64	25.2	*d*	*d*
CDV 75	2.04	21.9	*d*	*d*
CDV 76	2.70	28.2	*d*	*d*

[a] Estimates for FAST tests based on $V_{vessel} \approx 0.455\ m^3$.

[b] Tests at argon temperatures between 866 and 922 K.

[c] Values are approximate because voltage not accurately measured.

[d] No aerosol sampling done in vacuum tests.

[e] Capacitor discharge occurred for t > 20 msec, energy input calculated up to 9.25 msec.

output was collected and stored on the Nicolet digital storage oscilloscope and on magnetic tape using the data acquisition capability of a PDP/8A computer.

As in previous water tests, no fuel aerosol escaped from the water. The pressure trace output from the digital oscilloscope, shown in Fig. 1, indicates a large pulse occurring in ~60 msec and some other fairly large pulses occurring at t > 60 msec. However, after the test, it was determined that these were likely noise pulses produced by vibration of the transducer. (Tapping the transducer cable was found to create large voltage outputs.) Steps were taken to damp out possible vibrations for the next test.

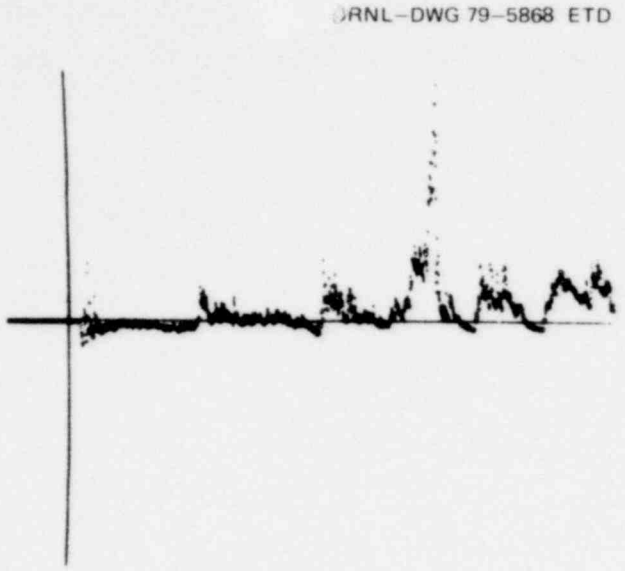

Fig. 1. Pressure transducer output collected on Nicolet digital oscilloscope for CDV 67; 100-msec total time; 1-V full-scale vertical deflection corresponds to 3000 psia.

It was also found that the PDP/8A computer data acquisition system (DAS) could not follow the rapid signal changes that occurred in this test (i.e., the computer circuitry does not have adequate frequency response to follow the pressure signals). For the FAST water tests, pressure data will be collected on a new digital oscilloscope that is being purchased.

CDV 68. Conditions for this test were the same as in CDV 67, where an effort was made to damp out possible pressure transducer (cable) vibrations. Again, no fuel escaped from the water following CDV, and pictures of the pressure transducer and capacitor discharge current output are shown in Figs. 2 and 3. Figure 2 indicates that transducer cable vibration problems seem to have been corrected. A pressure pulse occurred at 3.5 msec immediately after the CDV, shown in Fig. 3; the pulse was caused by the initial fuel burst. However, it is presently unclear why the transducer output became negative after the initial pulse.

To further understand the pressure signal that is measured, more underwater tests in CRI-III must be performed. These will be performed when the Sandia Normalization tests are completed and before FAST water tests begin.

ORNL-DWG 79-5869 ETD

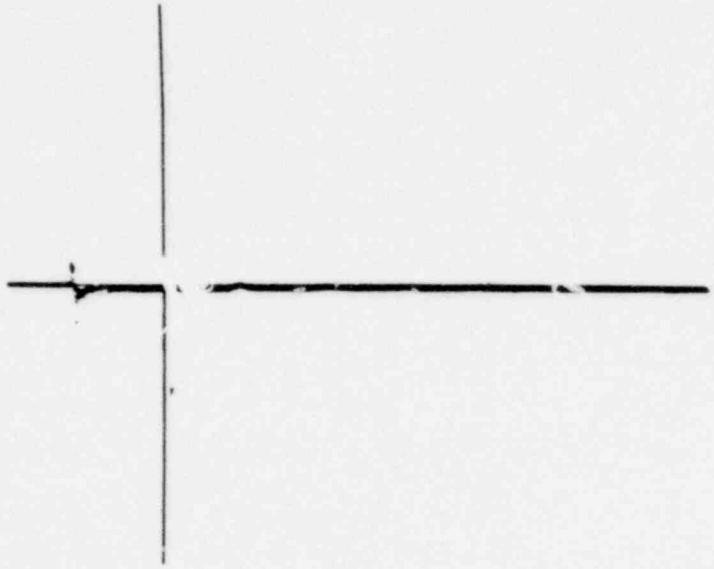

Fig. 2. Pressure transducer output collected on Nicolet digital oscilloscope for CDV 68; 200-msec total time; 1-V full-scale vertical deflection corresponds to 3000 psia.

ORNL-DWG 79-5870 ETD

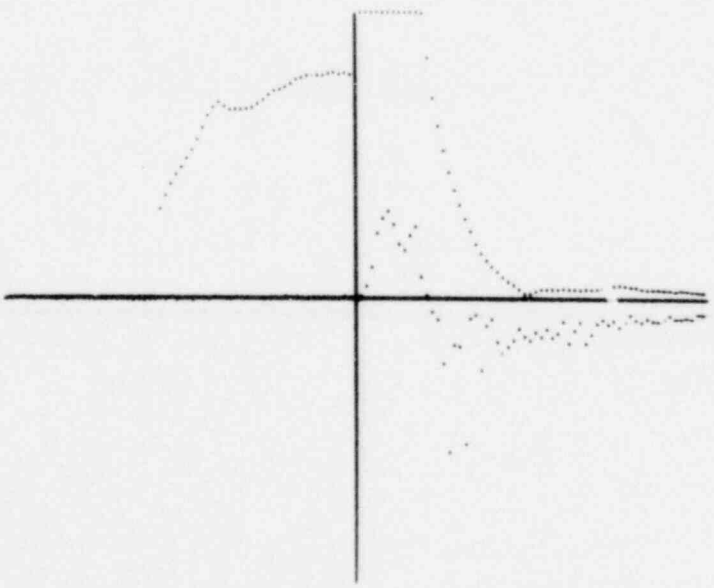

Fig. 3. CDV 68 current and pressure traces; time between data points is 100 μsec; peak pressure corresponds to ~240 psia; current at 3.5 msec is ~10,000 A.

2.1.3 Discussion of results from FAST high-temperature argon tests

The tests discussed in this section are the last to be performed as part of the FAST argon test series outlined in the FAST test plan.[2] Previous tests were performed at standard temperature and at 0.101- and 2.12-MPa (1- and 21-atm) argon pressures. The objectives of this test series are (1) to evaluate methods of making aerosol measurements at the extremes of pressure and temperature to be encountered in the later sodium tests and (2) to quantify the influence of argon pressure and temperature on the aerosol yield and primary aerosol size distribution produced.

FAST 12. Because this was the first time that the vessel was heated, 922 K (1200°F) was reached; adjustments in later tests allowed this temperature to be reduced to the planned 866 K (1100°F) level. At room temperature, the UO_2 sample resistance was 2.5 MΩ, but at 922 K the resistance decreased substantially to ~400 Ω. For the previous argon tests at room temperature, a 1700- to 1800-W high preheat was needed to produce a sample resistance of ~0.5 Ω, whereas for this test, a 1600-W high preheat produced a considerably lower (0.41-Ω) resistance. Capacitor discharge occurred for 1.57 msec, a shorter time period than expected. Measurements were made of aerosol concentration vs time (using the eight-stage mass sampler), and aerosol was collected onto tungsten photomicrograph grids mounted on diffusion plateout samples.

FAST 13. The test conditions were the same as those in FAST 12, except that the vessel temperature was at 866 K (1100°F). The vessel sight ports were maintained at 755 K (900°F) to reduce argon leakage through the port seals. The sample resistance at 866 K was 275 Ω, lower than the value at 922 K in FAST 12 (an indication that sample loadings are not always the same). Capacitor discharge occurred for 1.85 msec, a longer time than in FAST 12. As in FAST 12, aerosol mass concentration and aerosol plateout samples were taken.

FAST 14. This test was performed with the vessel maintained at 866 K (1100°F) and the sight ports held at 794 K (970°F). The sample resistance at 866 K was ~300 Ω, approximately the same as that in FAST 13. Capacitor bank charging voltage was reduced to 1850 V from the 1950-V values in FAST 12 and 13, in an attempt to increase the energy input time for capacitor

discharge. The energy input time of ~2 msec, however, was not considerably greater than in the other high-temperature tests. Aerosol mass concentration and plateout samples were again collected.

FAST 15. This was the final FAST test plan argon experiment, and was again performed at 866 K (1100°F). The sample resistance at 866 K was 1200 Ω, a factor of 4 higher than those of FAST 13 and 14. High preheat was reduced to 1500 W to produce a resistance of 0.5 Ω prior to capacitor discharge (the value usually achieved in low-temperature tests). Capacitor discharge occurred for 2.73 msec, ~1 msec longer than in the other high-temperature tests (this may have been caused by the reduced sample temperature resulting from lowering high preheat to 1500 W). Aerosol mass concentration and plateout samples were collected for this test.

A number of preliminary conclusions can be made concerning the high-temperature tests.

1. There were no major problems encountered in collecting fuel aerosol samples onto quartz-fiber filter-paper collection disks. It was found that the weight of the quartz disks decreased by 2 to 5% because of heating them to high temperatures. (This was done by weighing a blank filter before and after a test.) This weight loss is not significant for early-time mass measurements where the aerosol mass collected is large; however, it will become important for later-time mass measurements.

2. For a given preheat level, the sample resistance for high-temperature tests was lower than that produced in low temperature tests. This occurred for FAST 12 through 15 because the high temperature environment decreased the radiation loss from the fuel during steady-state preheat.

3. A comparison of aerosol yield vs capacitor discharge energy input, normalized to fuel pellet mass for all FAST argon tests, is presented in Fig. 4.

A comparison of results including the influence of varied sample preheats is being investigated. The graph indicates that less aerosol is produced for a given energy input at increased system pressure and that aerosol yields for 0.101-MPa pressure tests at high and low temperatures are similar. Both results were as expected, because fuel vaporization should cease when the fuel pressure equals the pressure of the surrounding argon.

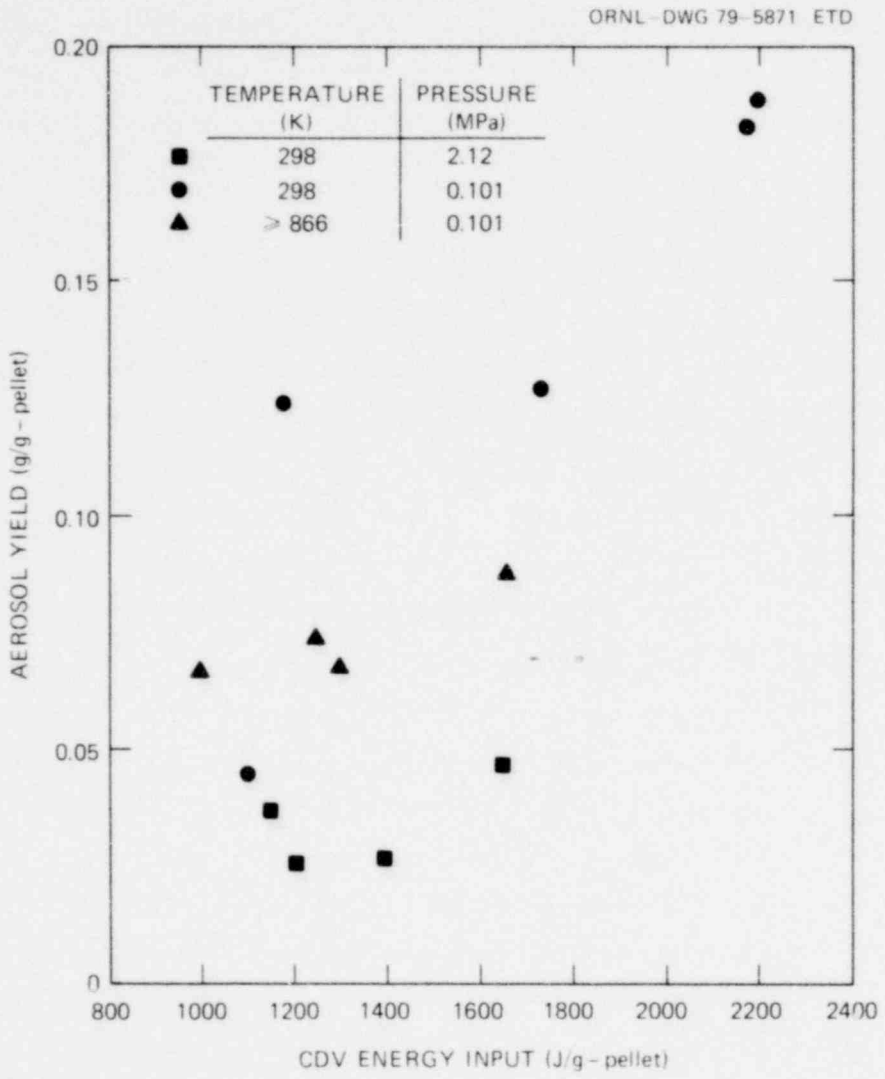

Fig. 4. Aerosol yield vs CDV energy input normalized to total fuel pellet mass for FAST argon tests.

FAST 16A. This was a special high-temperature test performed without the normal "preheat" stage. Based on an initial sample resistance for ~300 Ω at 866 K, simple calculations indicated that the test sample could be heated uniformly in ~250 msec to decrease resistance to ~10 Ω by discharge of one capacitor bank charged to 2500 V. Additional capacitor banks could then be discharged to heat the sample to vaporization conditions.

The use of this method as a more efficient vaporization technique for high-temperature tests could not be determined, because arcing terminated

the test before any energy was input to the sample. Further investigation to determine the potential of this method will continue.

After this test, preparations were made to begin water tests early next quarter.

2.1.4 Discussion of vacuum tests performed in CRI-III

The Sandia Normalization tests are CRI-III experiments performed at low vessel pressure (~100 μ Hg). The UO_2 debris produced by CDV will be sampled using a rotating wheel collector developed at Sandia to allow determination of droplet sizes and velocities. These measurements will allow comparison of debris, produced at comparable energy levels, using electrical (CDV) energy input and neutronic energy input [in Sandia's Annular Core Research Reactor (ACRR)].

Movies will be taken during fuel heatup and the fuel radiance that results in film exposure will be used to determine fuel temperature. Various configurations (discussed later) will be used to expose portions of the fuel pellets, and this may allow surface temperature measurements to be made.

The first three tests discussed, CDV 69 through 71, were in preparation for the Sandia tests. Tests CDV 72 through 76 were the first five in the Sandia Normalization test series.

CDV 69. In CDV 57, the only previously successful vacuum test, six banks were charged to 1600 V, and CDV energy input occurred for more than 18 msec. In CDV 69, four banks at 1950 V, the normal changing configuration, was used because the arcing problems had been eliminated. The initial vessel pressure before preheat was 105 μm Hg. No problems were encountered during preheat start-up (performed at voltages greater than 2000 V) or during the low- and high-preheat stages. Capacitor discharge was successful and occurred for 2.4 msec. The discharge was somewhat different than that normally produced in argon; the CDV current continually increased with time, whereas, in argon, it usually flattens out after 1 to 2 msec of discharge before increasing again. As in CDV 57, all sight ports were immediately coated with fuel after CDV.

CDV 70A. For this test, the charging voltage was reduced to 1850 V in an attempt to lengthen the CDV energy input time; however, the decrease

in changing voltage resulted in an energy input time of >20 msec. The decreased rate of energy input may account for partial melting of the low-voltage electrode that was observed in posttest examination of the sample. Based on this test, future vacuum tests will be performed with four banks charged to 1950 V.

CDV 71. The capacitors were charged to 1950 V. Preheat occurred without any problems, and the high energy input caused by the 7.36-msec energy input time made this the most successful vacuum test to date.

The five tests performed during the remainder of this quarter were the first five Sandia Normalization tests. (R. M. Elrick and D. L. Fastle from Sandia Laboratories assisted with these experiments.) Figure 5 shows the mount used to house the rotating wheel sampler in the CRI-III vessel. The sampling wheel contains 30 pie-shaped channels that have surfaces prepared for examination under scanning- and transmission-electron microscopes; it is housed in the cover shown at the lower end of the sample mount. The mount is inserted through the top port of CRI-III so that the wheel is positioned a ~4.45 cm (1.75 in.) above the radial centerline of the fuel sample. Particles enter the sampling wheel, which is rotated at speeds between 200 and 400 rps, through a small slit in the sample cover. Small steel pins are implated into the back flat surface of the wheel; recording of signals from a magnetic pickup exposed to this wheel surface enables the rotation speed to be determined.

CDV 72 (SN-1). For this first Sandia test, a specially designed quartz tube was used to house the UO_2 fuel sample, as shown in Figs. 6 and 7. The close-up in Fig. 7 shows that a portion of a pellet (~0.64 cm or 0.25 in. in length) is exposed by reducing the inner diameter of the quartz tube in this section. This pellet has a 0.16-cm (0.064-in.) hole drilled to its center. Close-up movies taken of this pellet section will be examined with a densitometer to see if it is possible to determine surface and centerline temperatures or, at least, to determine their ratio.

The sampling wheel cover slit was 0.038 cm (0.015 in.) to keep microspheres (which have diameters greater than 0.035 cm) from penetrating to the wheel surfaces. Two cameras were used to photograph the event: one for a close-up of the fuel pellet and the other for a full field view of the sample. Only the camera used for the latter purpose operated correctly in this test.

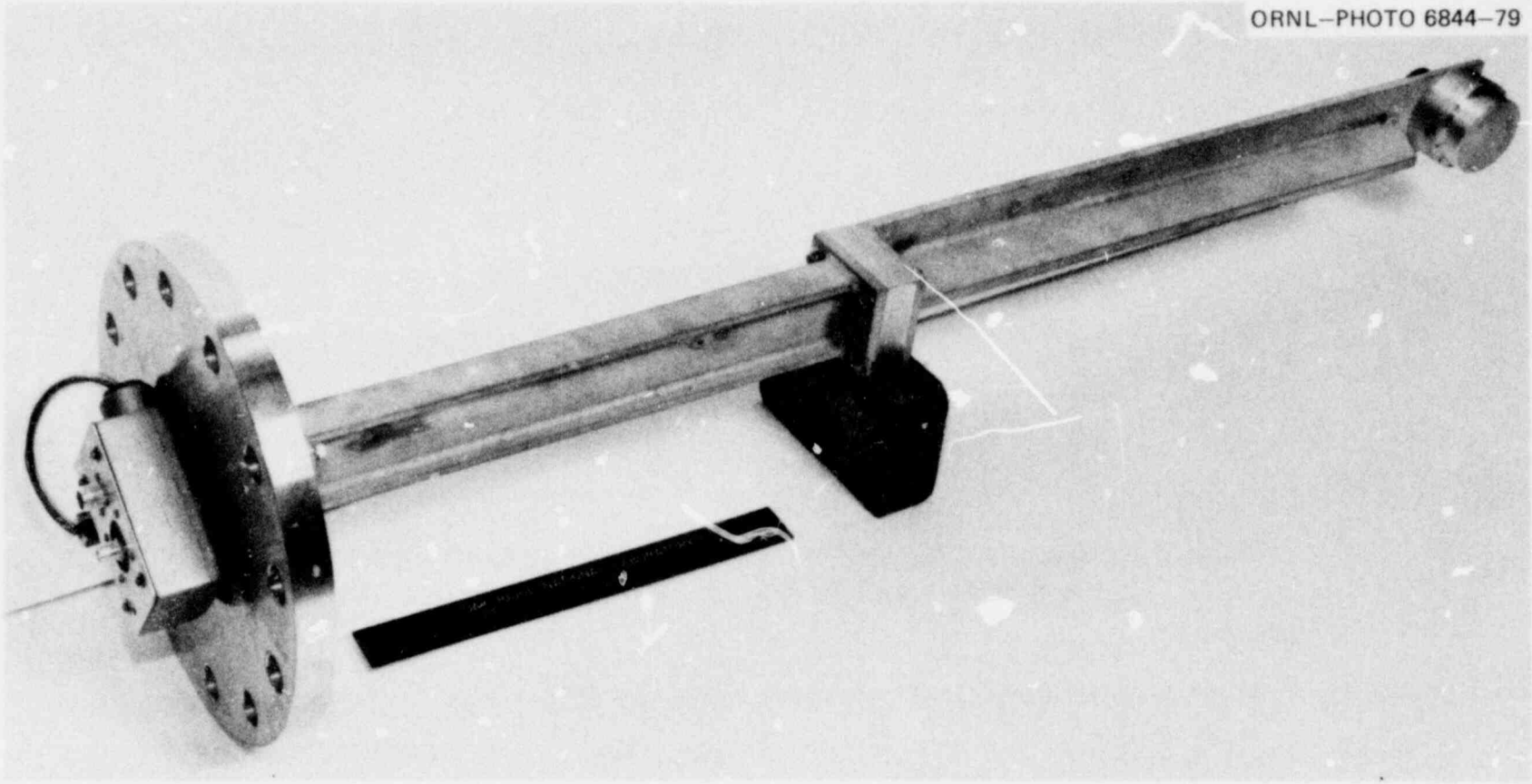

Fig. 5. View of support structure, sample wheel assembly, and associated control box for rotating sample wheel mount used in Sandia vacuum tests.

ORNL-PHOTO 6846-79

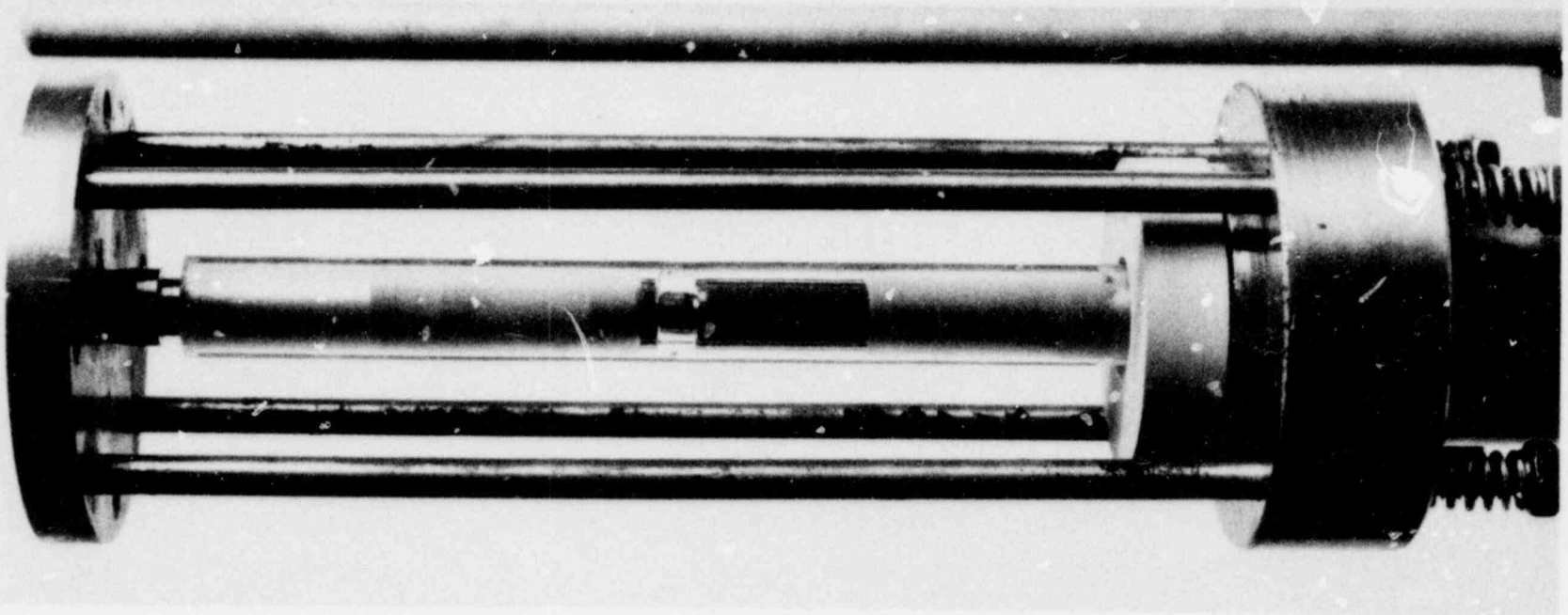

Fig. 6. View of vaporizer assembly used in CDV tests 72 through 74 showing quartz tube, low-voltage electrode, and pellet stack and microsphere assembly. Exposed UO_2 pellet with hole in center is also shown.

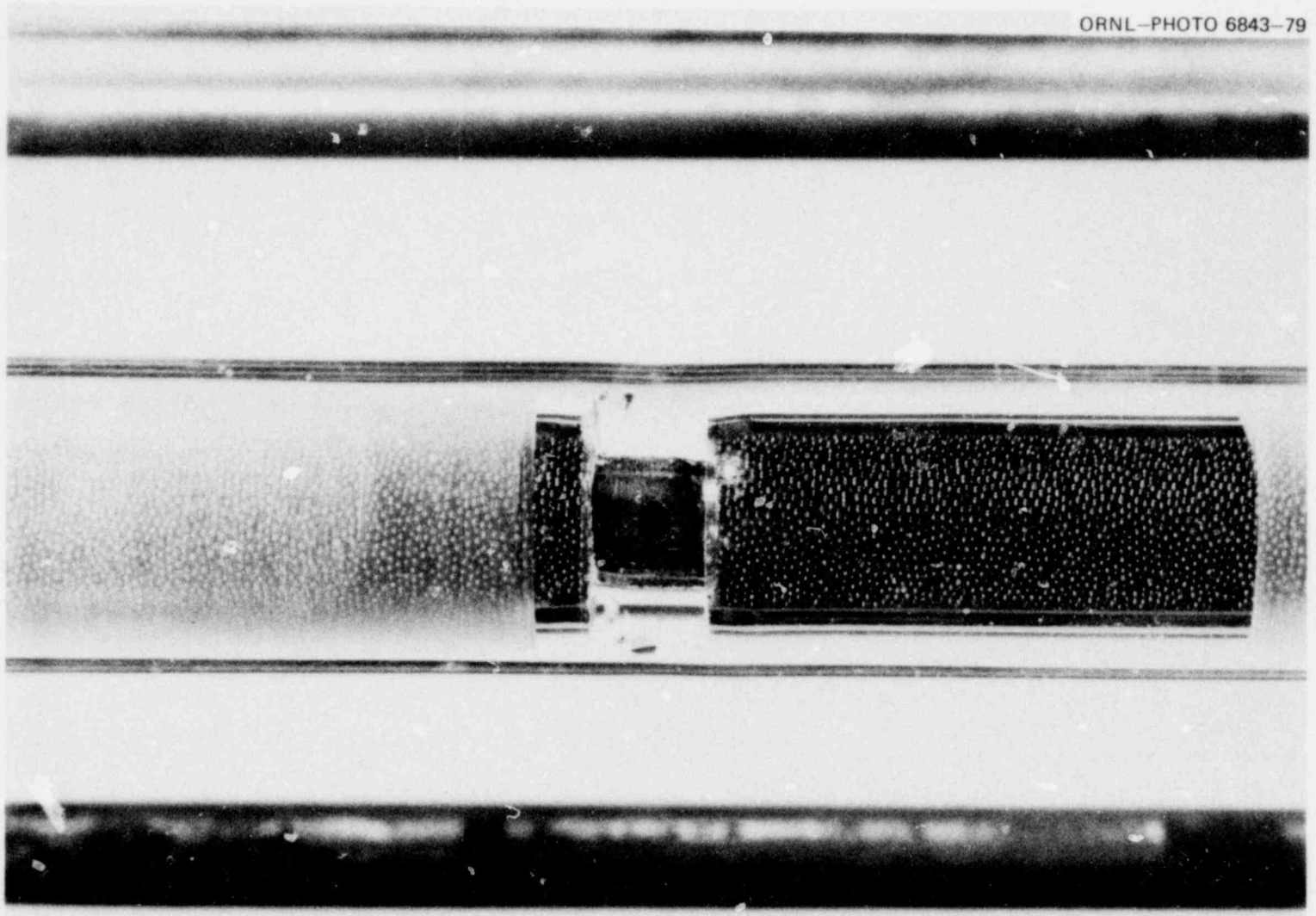

Fig. 7. Close-up of quartz tube assembly for CDV tests 72 through 74 showing exposed UO_2 with 1/16-in.-diam hole bored to center of pellet and UO_2 microspheres surrounding remainder of pellet stack.

Preheat and capacitor discharge occurred as expected. During early preheat (at ~200 W), the hole in the pellet glowed brighter than the pellet surface indicating the hotter centerline temperature. The wheel was rotated during discharge at ~400 rps, or one revolution in 2.5 msec.

Posttest examination of the sampling wheel provided no clear evidence of fuel deposit onto the wheel.

CDV 73 (SN-2). Conditions for this test were the same as for CDV 72, except that a wider wheel cover slit of 0.064 cm (0.025 in.) was used. This was done to promote more penetration of debris to the wheel surfaces.

Preheat went smoothly, but arcing occurred at 0.22 msec after discharge began, and the test was thus terminated. This occurred because one of the lavite insulators in the test assembly cracked prematurely, allowing arcing to occur between the inner copper electrode and the steel housing of the assembly. The quartz tube did not rupture, so the sampling wheel mounted for this test was used again in CDV 74.

CDV 74 (SN-3). Conditions for CDV 74 were the same as in test 73, where a quartz tube with a reduced diameter section was also used to allow pellet exposure. The CDV energy input of 25.2 kJ was considerably larger than that in CDV 72. The sampling wheel rotation speed was ~250 rps, about half that in CDV 72. The viewports were covered with fuel after the test, but, again, there was little direct visual evidence of collection of debris onto the outer circumference of the wheel. Most of the debris collection, however, should occur deep inside the wheel on the pie-shaped collection surfaces that were not visible. Both cameras worked well during the test.

CDV 75 (SN-4). The quartz tube used for this test had no reduced diameter section, but it did have a clear central section to allow movies to be made of the microsphere surface. The slit was widened considerably to 0.198 cm (0.078 in.) to enhance debris collection onto sampling wheel collection surfaces. One camera was used for a close-up of a microsphere section, the other for a full-field view of the sample.

Preheat and capacitor bank charging conditions were the same as in CDV 72 and 74. Discharge occurred for 2.04 msec, a period which was again shorter than expected. As in CDV 69, the CDV current (for reasons yet

unknown) continually increased with time (and usually stopped increasing somewhere between 1 to 2 msec). The final wheel speed achieved was 400 rps. Both cameras again operated properly.

Examination of the surface of the wheel cover after the test showed that it was well coated with fuel. There was some possible evidence of debris collection on the wheel; the wheel circumference appeared sand-blasted, and holes were evident in some of the collection surfaces.

CDV 76 (SN-5). This was the first test in which a different configuration was used to view a portion of a pellet (shown in Figs. 8 and 9). A small alumina viewing slit was glued to the inner tube surface; this allowed a sector of a pellet containing a 0.16-cm (0.065-in.) hole to be exposed. The wheel cover slit width was reduced slightly for this test, to 0.127 cm (0.050 in.). Preheat and bank charging were again maintained at the same levels used in CDV 72, 74, and 75. One camera was used for a pellet close-up, the other camera for a full-field view of the sample.

During early preheat (~300 W) it was again observed that the hole in the pellet looked brighter than the pellet surface. A few seconds into high preheat, there was evidence from both visualization and the preheat power trace indicating that the alumina window cracked and/or closed up due to melting. In spite of this problem, the CDV input energy was the largest attained in the Sandia tests performed to date. The wheel rotation speed achieved was ~300 rps, and both cameras operated properly for this test.

After CDV, the viewports were totally covered with fuel, as was the cover for the sampling wheel. This may be the best indication that debris was collected onto the wheel surfaces.

Summary and comments for first five Sandia Normalization tests. For the tests performed to date, the CDV energy inputs ranged from ~18 to 28 kJ. The only "missing link" now is an experiment with an energy input in the 40-kJ range. Tests were performed (1) with a variety of configurations to expose different portions of a pellet for temperature measurement, and (2) with a wide range of wheel cover slit openings and various wheel rotation speeds for fuel debris collection.

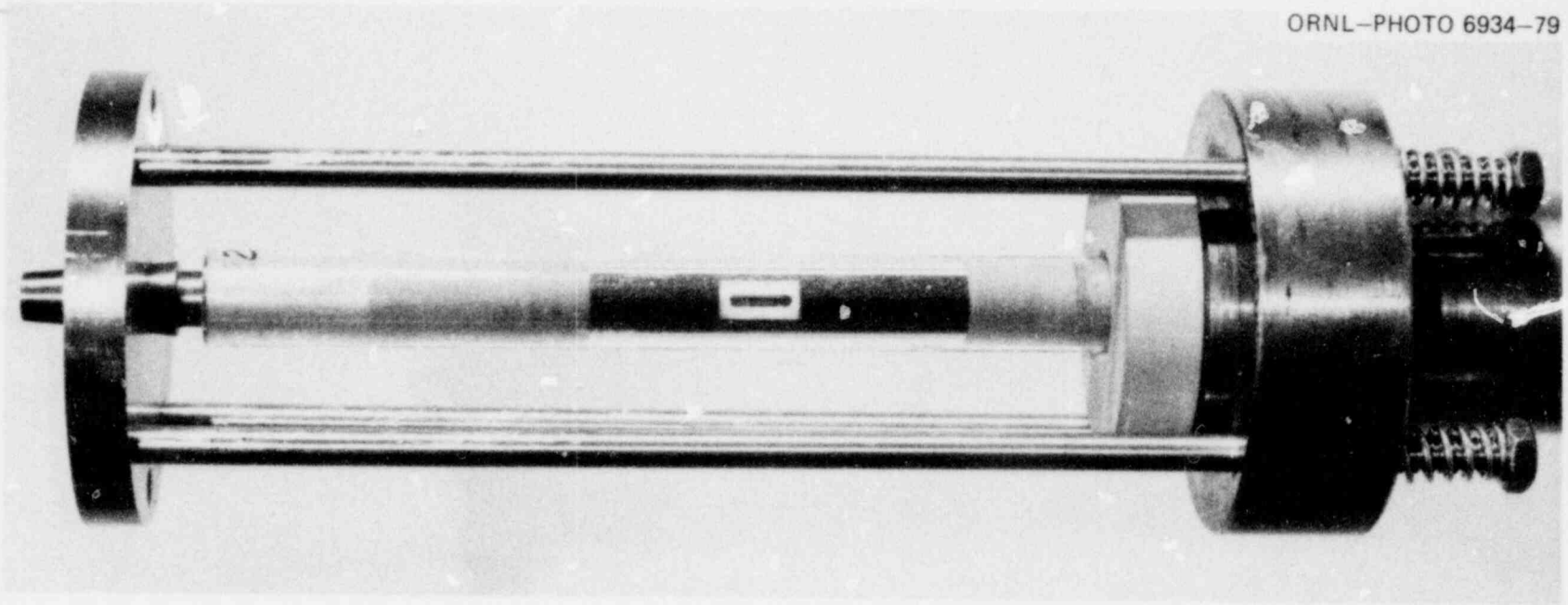

Fig. 8. View of type of vaporizer assembly used in CDV 76 showing quartz tube, low-voltage electrode, UO_2 microspheres surrounding UO_2 pellet stack, and bare side of UO_2 pellet as viewed through Al_2O_3 "window" glued to ID of quartz tube.

ORNL-PHOTO 6933-79

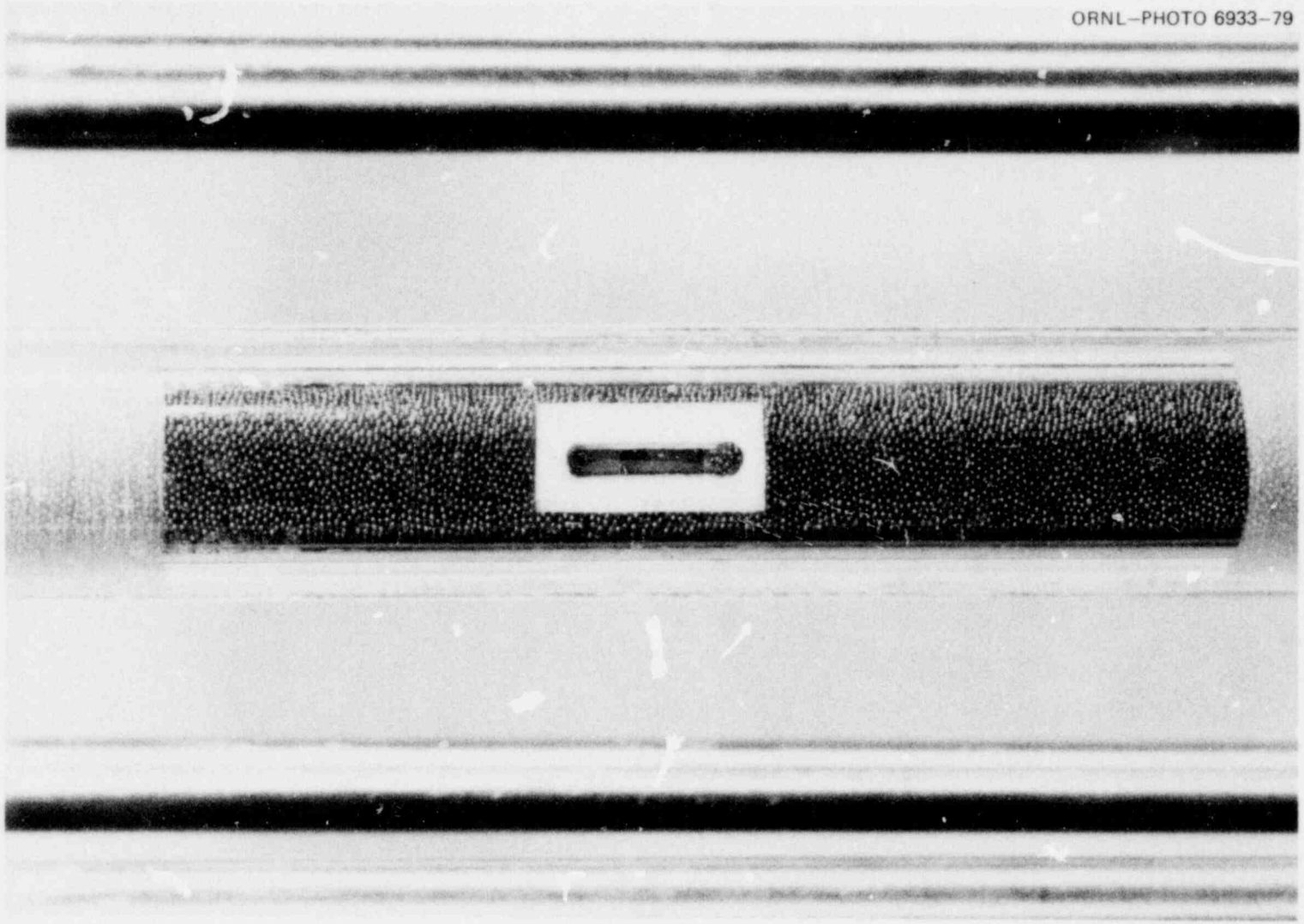

Fig. 9. Close-up view of sample assembly used in CDV 76 showing Al_2O_3 window glued to ID of tube, exposed side of UO_2 pellet with a 1/16-in.-diam hole, and UO_2 microspheres surrounding rest of pellet stack.

Two more experiments will be performed next quarter. Another test with a sampling wheel in the vessel will be performed so that a high-energy input can be achieved. In the final test, movies will be made for the latter stage of low preheat, the 28-sec high preheat, and sample cool-down after high preheat. Temperature measurements will be made from the films to gain a better understanding of the fuel temperatures achieved before CDV.

2.2 Secondary Containment Aerosol Studies in NSPP

R. E. Adams L. F. Parsly

2.2.1 Introduction

Activities of the NSPP during this period were primarily concerned with installation and preliminary checkout of the new dc plasma torch uranium oxide aerosol generator.

2.2.2 dc plasma torch uranium oxide aerosol generator

This generator, developed by another group within the ART Program,[3] has been adapted to the NSPP system. The generator is composed of a METCO Model 7M plasma flame spray system and a special water-cooled combustion adapter head through which uranium powder and oxygen gas are added to the argon plasma flame to produce an aerosol of uranium oxide (U_3O_8). Figure 10 is a photo of the METCO plasma flame system, which is composed of, from left to right, a power supply, control cabinet, heat exchanger, powder feed unit, and the plasma torch. The METCO plasma torch fitted with the special adapter head and powder feed system is shown during operation in Fig. 11.

Space constraints at the NSPP required that the power supply, control cabinet, and heat exchanger be installed in one area. The powder feed unit (contained in a vacuum glove box under an argon environment) was installed near the vessel, and the plasma torch, including the adapter, was mounted on the vessel wall. Some function switches on the control cabinet are duplicated in a remote panel in the NSPP control room. Generation of aerosol with this system requires three operators — one in the NSPP control room, one at the plasma torch control cabinet, and one at the vacuum glove box/plasma torch installation site.

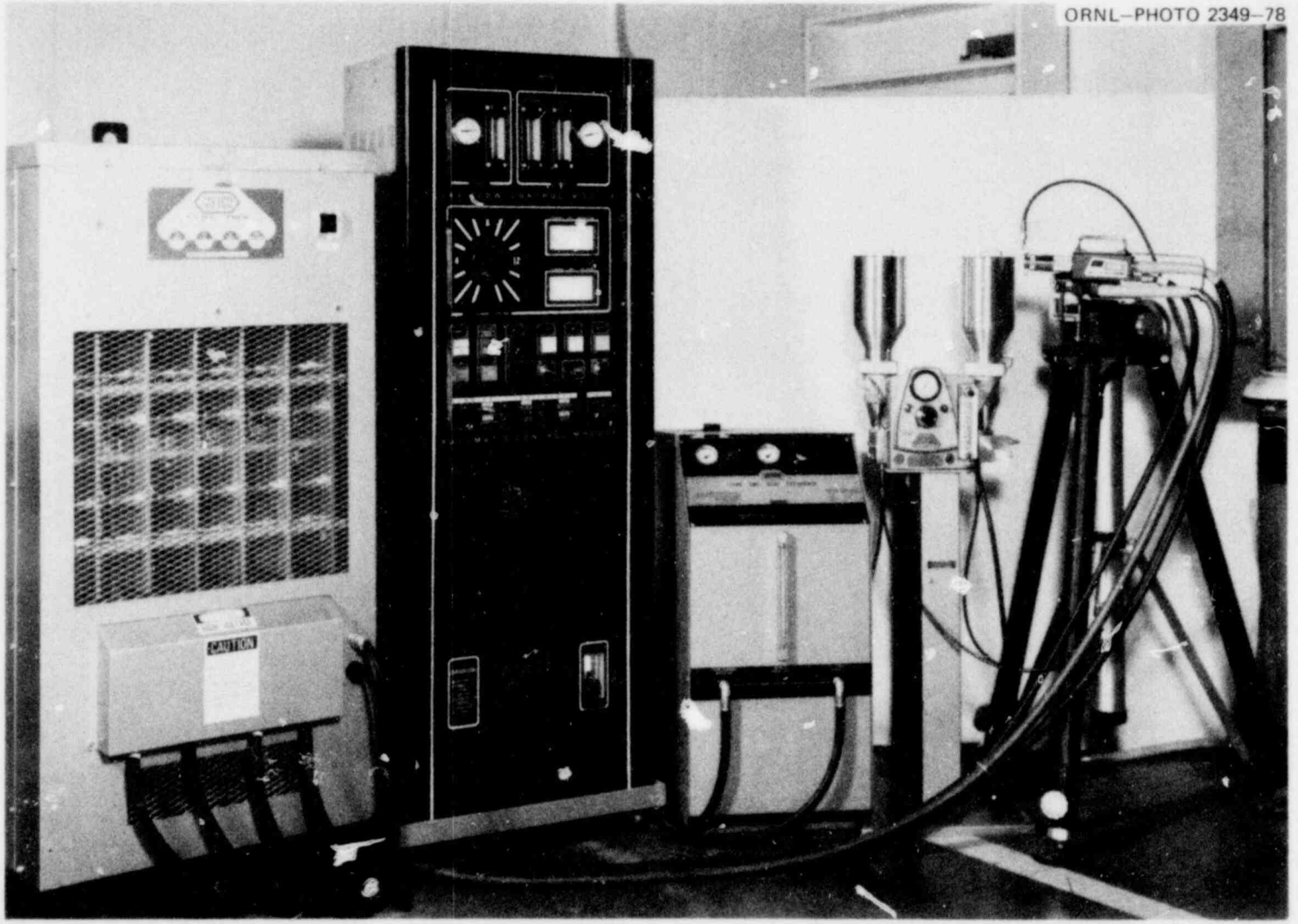

Fig. 10. Component parts of METCO Model 7M plasma flame spray system.

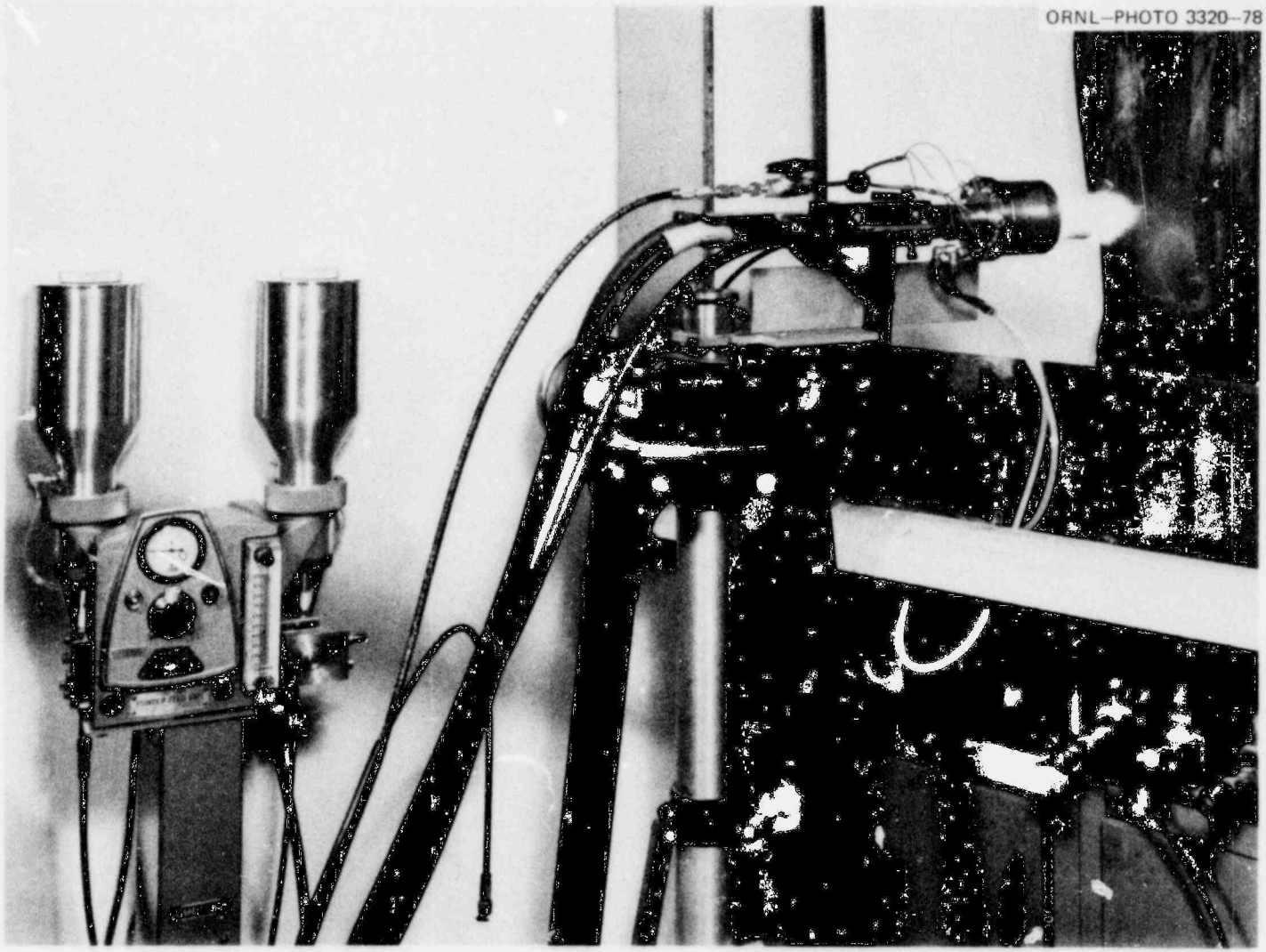

Fig. 11. METCO plasma torch fitted with special adapter head for burning uranium metal powder.

2.2.3 Preliminary aerosol generation tests

After electrical and control function testing, one aerosol generation test was made by introducing iron powder into the torch generator. After several minutes of aerosol generation with an abundant amount of aerosol produced, the powder feed system gave indications of plugging. After termination of the test, inspection of the adapter head revealed that several of the capillary tubes had been plugged with an iron slag. These obstructions were removed, and the adapte head was cleaned in preparation for the first uranium oxide generation test.

The first uranium test (run 204) was to use 500 g of uranium powder as source material. Powder feed problems occurred very early in the generation period. The plasma torch operated for about 23 min, but only a very small quantity of uranium powder reached the adapter head. Visual observation of the vessel interior revealed that the uranium oxide aerosol concentration was very low; therefore, the run was terminated and no aerosol samples were taken. It was shown that the torch and adapter head could be operated for a long period of time without any apparent damage to the equipment by the high-temperature plasma flame. Posttest examination of the adapter head revealed some plugging of the capillary powder feed tubes. However, the major source of the powder feed problem was with the feeder unit and the primary powder feed tubing. The very fine uranium powder appeared to be packed within the powder hopper, thus restricting its flow into the powder feed wheel. Also, the powder feed tubing was installed such that the powder had to be raised in elevation before reaching the adapter head, thus causing a large amount of powder to accumulate in the low point of the tubing.

Before the second attempt to perform run 204, the powder feed unit was cleaned and the powder feed tubing replaced with a slightly smaller-diameter tube arranged so that the exit from the powder feeder was higher than the entry to the adapter head. In addition, all capillary tubing in the adapter head was replaced with new tubing. The second attempt was partially successful, even though uranium powder plugging was again encountered within the powder hopper and powder wheel area. The torch was operated for about 20 min, although most of the aerosol production occurred in the first few minutes. Visual observation indicated sufficient

aerosol production to allow the run to be carried out as planned, with aerosol samples taken for 48 hr. All results from the analytical lab have not been received at this time; however, an estimate of aerosol mass concentration from the cascade impactor data indicates that a maximum concentration approaching 1 g/m^3 was achieved. The behavior of this aerosol produced by the plasma generator will be compared with that of the lower-concentration aerosol produced by the consummable electrode aerosol generator (runs 201 through 203).

2.2.4 Future uranium oxide aerosol tests

It appears that the powder feed problems were caused by the very small particle size of the uranium powder (<40 μm). Before the next aerosol test, uranium powder of a larger particle size will be obtained. In addition, operation of the powder feeder will be studied with tungsten powder as a substitute for uranium powder.

2.3 Basic Aerosol Experiments in CRI-II

G. W. Parker A. L. Sutton, Jr.

2.3.1 Fuel aerosol particle size measurement

As part of an effort to evaluate aerosol size measuring techniques and instrumentation in use in LMFBR safety studies, the long-duct spiral aerosol centrifuge (Stober design) has been applied repeatedly to the U_3O_8 (metal oxygen combustion) high-density aerosol in the CRI-II facility. The results have shown excellent precision and reproducibility; however, they tend to disagree significantly with the measurements obtained from inertial cascade impactors such as the Andersen 400 jet nonviable model. The suspected cause for the consistent disagreement is that the nature of the fuel aerosols (long branched chains) leads to fracturing by the impactor jets.

In the previous quarterly report,[1] a comparison of the U_3O_8 agglomerate size measurements for run PT-19 was made showing the discrepancy between the centrifuge measurements and the cascade impactor measurements. Similar results were obtained from additional comparisons using size distribution data for runs PT-22 and 24, which had initial U_3O_8

aerosol concentrations of about 20 to 40 g/m^3, as shown in Figs. 12 and 13.

To test the impactor for wall losses that might contribute to the factor of two lower apparent sizes measured by the impactor, alternate samples were taken on silicone oil-coated plates and compared with the data from the usual filter-paper collectors. No significant difference was observed between these two collector surfaces, thus diminishing the effect due to wall losses.

A similar observation on PuO_2—UO_2 vapor-condensation aerosols has been reported by Raabe.[4] When he compared sizes of particles measured by the Lovelace Centrifuge [operated at Los Alamos Scientific Laboratory (LASL)] with those derived by an impactor, he concluded simply that impactor samples were always smaller in diameter than those obtained with the centrifuge.

The photograph in Fig. 14 shows the two types of cascade impactor plates (oil and paper). The apparent concentrations around plates 4 and 5 indicate that the usual aerodynamic mass median diameter (AMMD) measured by this method is about half the centrifuge value.

Thus, previous measurements made by the impactors on UO_2 (arc-furnace) aerosol are questionable, and the tests should be repeated using the spiral centrifuge. One such test has been completed with approximately the same results as with the U_3O_8 aerosol. Maximum particle diameters were ~14 μ, compared to about 12 μ for U_3O_8 aerosol. This was at a significantly lower maximum concentration, which tends to agree with the extra bulk density of UO_2 vs U_3O_8. These comparative measurements are to be continued with both Na_2O and mixed U_3O_8-Na_2O_x aerosols generated in the NSPP tests and with the more finely subdivided UO_2 generated in the CDV/CRI-III tests.

In the two photographs in Fig. 15, the relative deposition profiles for U_3O_8 oxide (run PT-19) and UO_2 oxide (run AF-11) are compared to illustrate the nearly identical size distribution. The AMMDs for run PT-19 were about 6.5 μm; analytical results not yet obtained for run AF-11 are expected to be nearly the same or slightly larger than 6.5 μm.

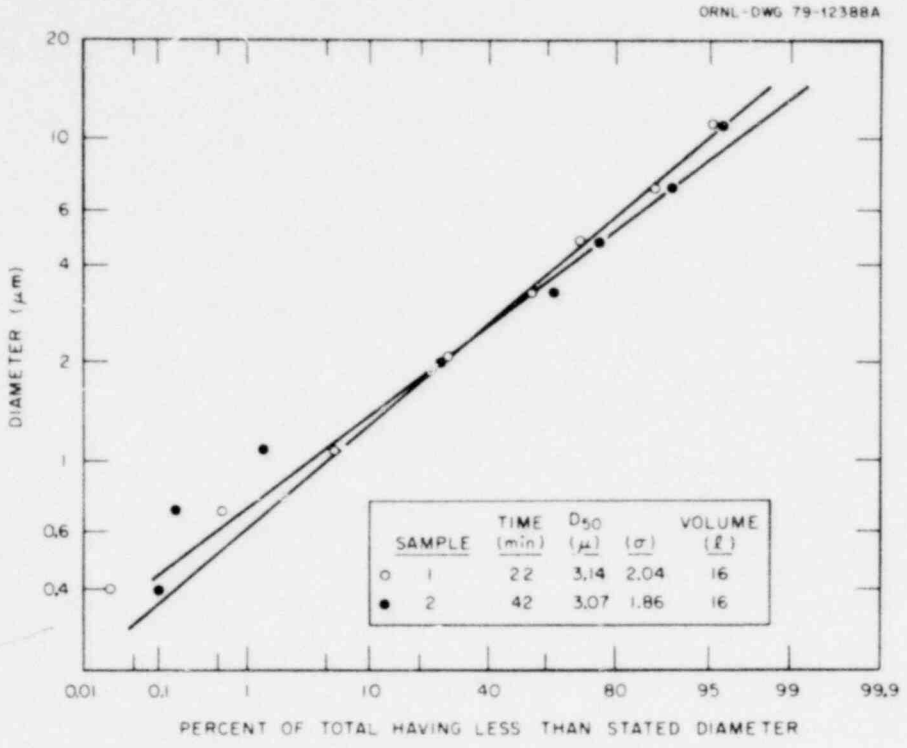

(a) PLASMA TORCH RUN 22 IMPACTOR SAMPLES

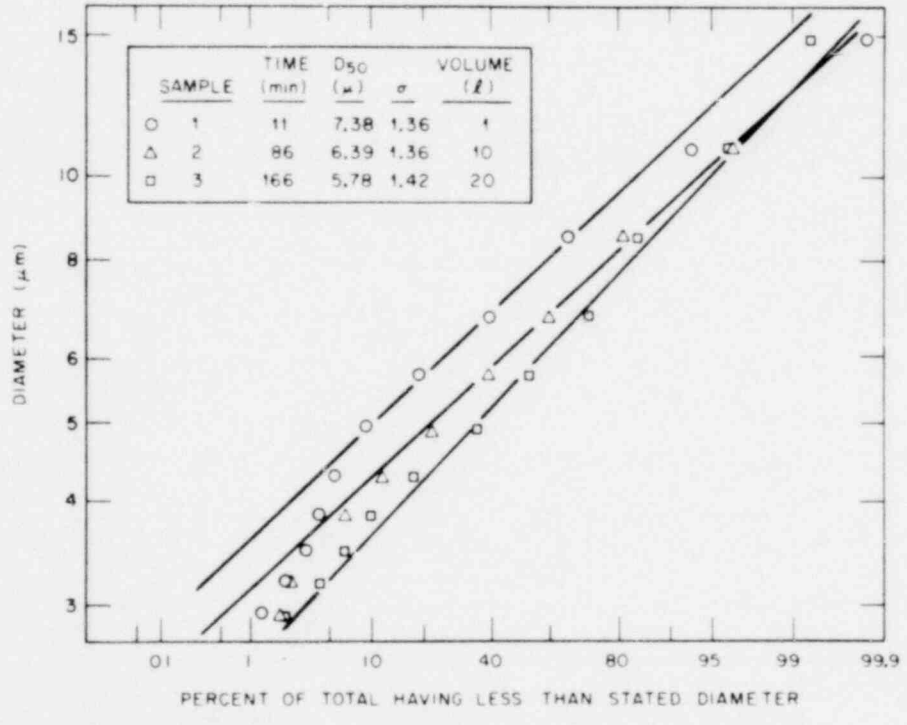

(b) PLASMA TORCH RUN 22 SPIRAL CENTRIFUGE

Fig. 12. Comparison of impactor-measured aerodynamic diameters with spiral centrifuge diameters for run PT-22.

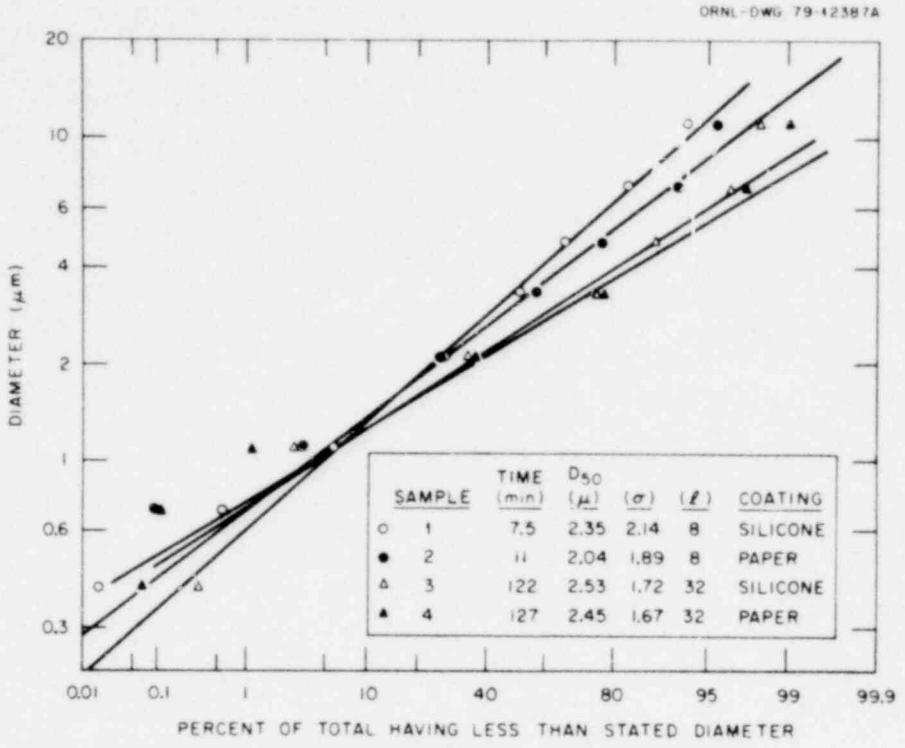

(a) PLASMA TORCH RUN 24 IMPACTOR SAMPLES

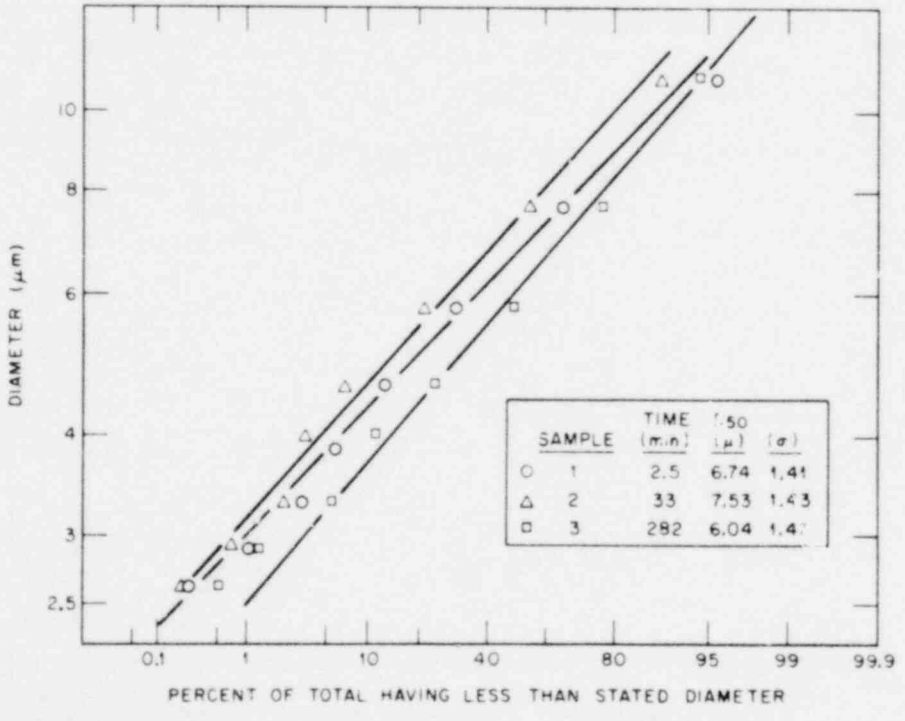

(b) PLASMA TORCH RUN 24 SPIRAL CENTRIFUGE

Fig. 13. Comparison of impactor-measured aerodynamic diameters with spiral centrifuge diameters for run PT-24.

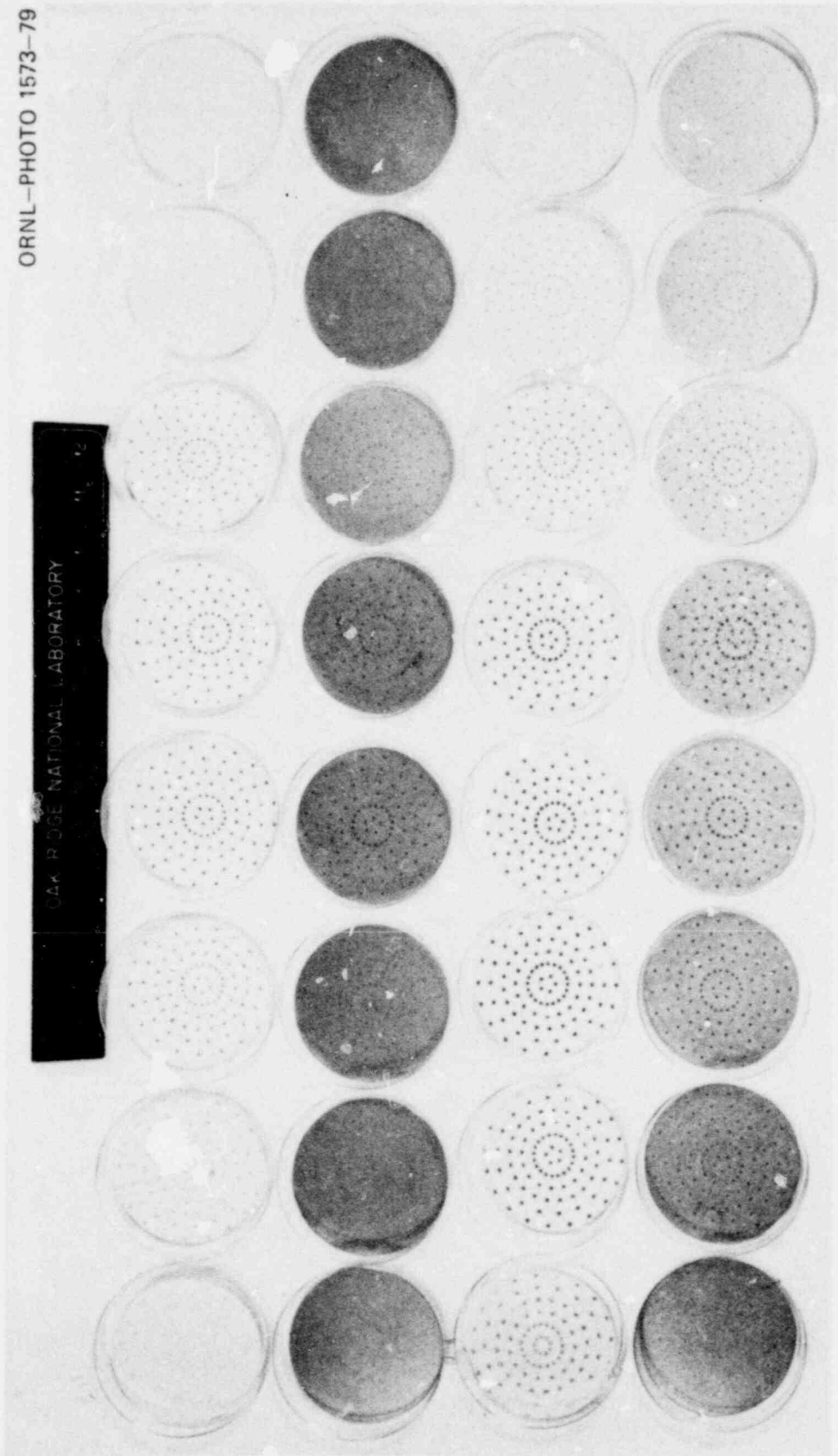

Fig. 14. Appearance of UO_2 on two types of collector surfaces (oil and paper) from cascade impactor.

ORNL-DWG 79-539A

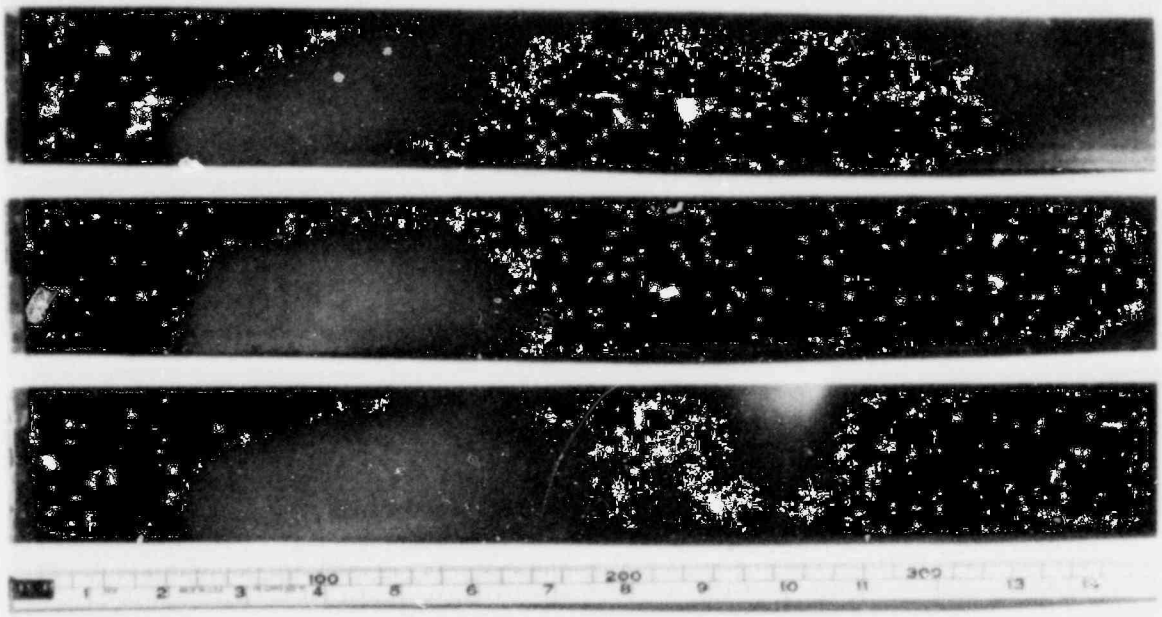

(a) DISTRIBUTION OF UO_2 PARTICLES FROM RUN AF-11

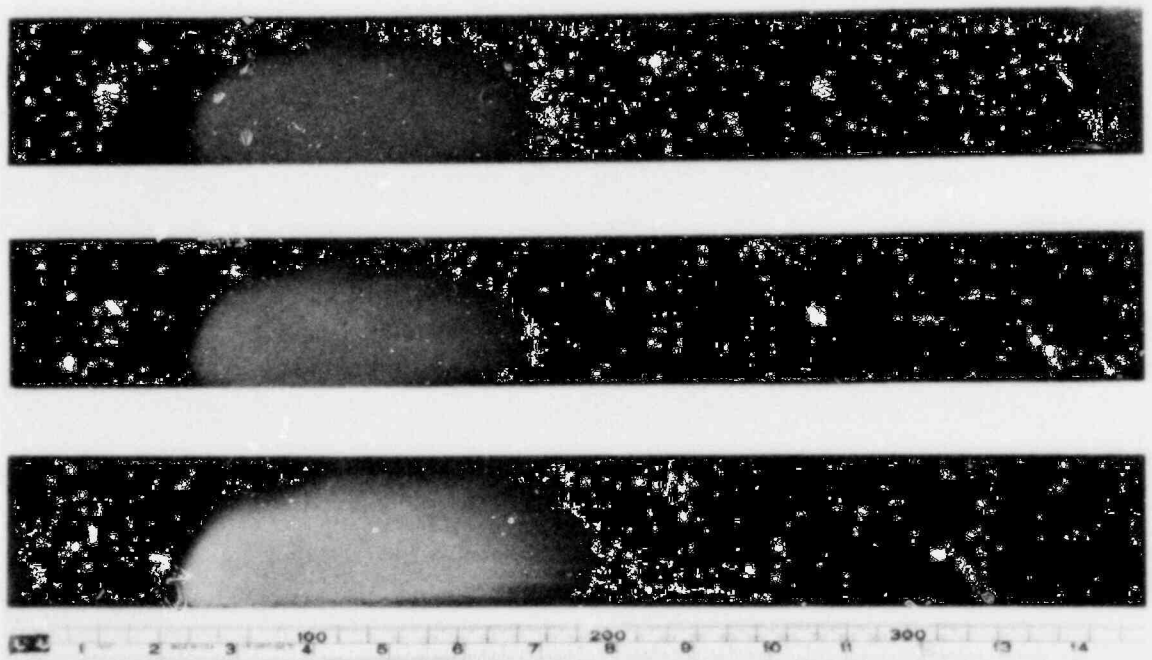

(b) DISTRIBUTION OF U_3O_8 PARTICLES FROM RUN PT-19

Fig. 15. Appearance of centrifuge collector foils for (a) UO_2 and (b) U_3O_8.

2.3.2 Size of aerosol agglomerates calculated from experimental data

Using the observed condensation nuclei count (Fig. 16), the airborne mass concentration (Fig. 17), and the average primary particle diameter derived from the BET surface area measurements of the settled aerosol, a sample calculation has been performed to obtain an "effective" agglomerate diameter.

From the condensation nuclei count (Fig. 16), we have

$$N = 4 \times 10^{9}\, e^{-0.484t} + 1.1 \times 10^{5}\, e^{-6.9 \times 10^{-3} t} . \qquad (2.1)$$

In the above equation, the initial value of N, 4×10^{9}, is calculated from the initial aerosol mass concentration (C = 20.15 μg/mℓ at t = 0) and the initial primary particle diameter ($D = 1.05 \times 10^{-5}$ cm at t = 0), which was determined from BET surface area. By the definition of the effective diameter, we have

$$N\rho \left(\frac{\pi D^3}{6}\right) = C \times 10^{-6} , \qquad (2.2)$$

where D is effective diameter and C is aerosol mass concentration in μg/mℓ.

$$N = \frac{C(6 \times 10^{-6})}{\rho \pi D^3} = \frac{20.15(6 \times 10^{-6})}{8.3\pi(1.05 \times 10^{-5})^3} = 4 \times 10^{9} . \qquad (2.3)$$

From the airborne mass concentration data (Fig. 17), we have

$$C = 17\, e^{-0.0871t} + 3.15\, e^{-0.0162t} , \qquad (2.4)$$

where t is in minutes. Substituting Eq. (2.2) into the equation above

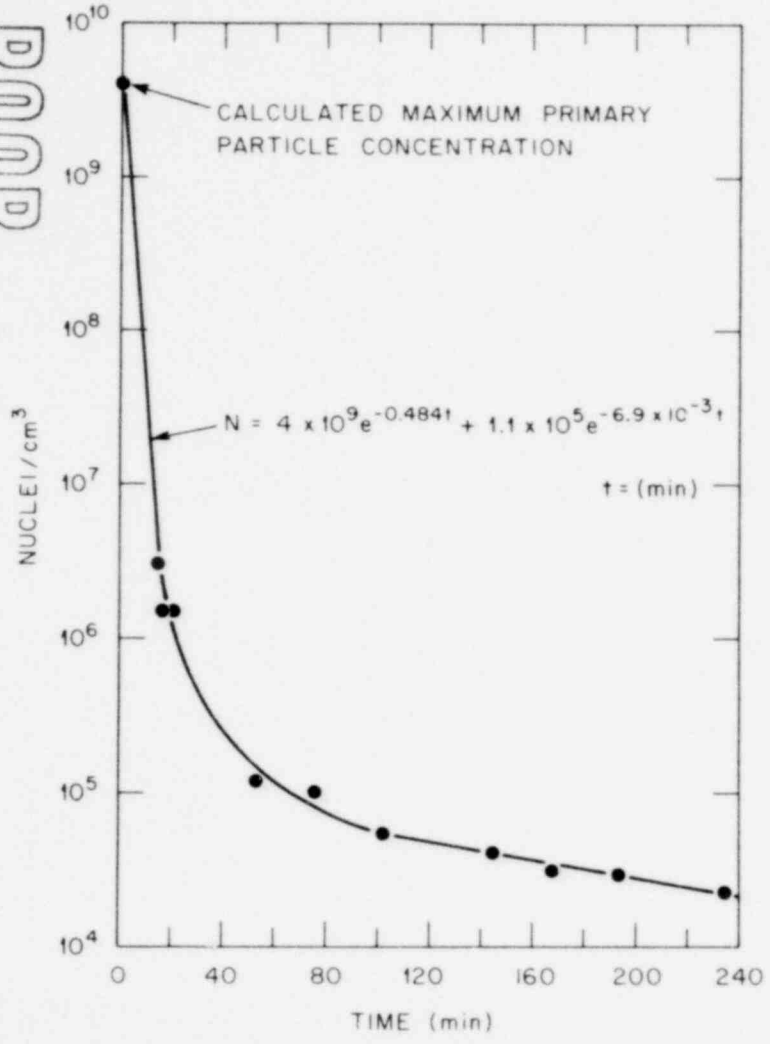

Fig. 16. Change in condensation nuclei count for run PT-22.

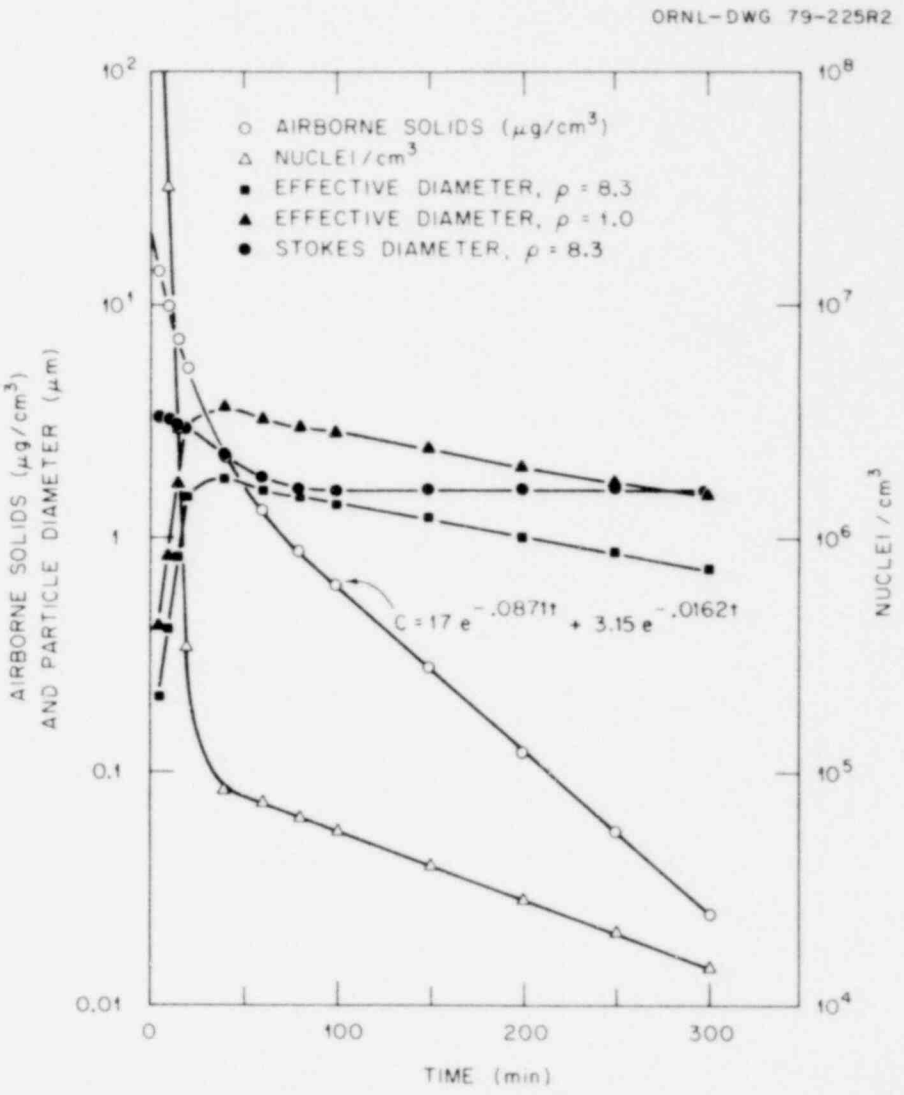

Fig. 17. Particle sizes calculated from number concentration and airborne mass concentration for run PT-22.

yields

$$D = \sqrt[3]{\frac{(6 \times 10^{-6})C}{N\pi\rho}} \tag{2.5}$$

$$D = \sqrt[3]{\frac{1.91 \times 10^{-6}}{\rho}\left[\frac{17\, e^{-0.0871t} + 3.15\, e^{-0.0162t}}{4 \times 10^{9}\, e^{-0.484t} + \left(1.1 \times 10^{5}\, e^{-6.9 \times 10^{-3}t}\right)}\right]}.$$

The effective particle diameter results are listed in Table 4 using selected values of ρ of both 8.3 and 1.0 gm/cm^3. The theoretical or bulk density (8.3 for U_3O_8) has no real meaning in the calculation, because the shape, fluffiness, and large void volumes between chains and branches make the aerosol behavior dependent on the exact nature of these properties, which are presently not measured. However, with ρ = 1, the calculated effective diameter is in fair agreement with the measured impactor diameters, whereas Stokes diameters more nearly confirm the centrifuge data.

Table 4. Calculated effective particle diameters of U_3O_8 agglomerates

Time (min)	Nuclei (cm^{-3})	C (μg/mℓ)	D[a] (μ)	D[b] (μ)
5	3.6×10^8	13.9	0.21	0.42
10	3.2×10^7	9.8	0.41	0.83
15	2.9×10^6	7.1	0.82	1.7
20	3.4×10^5	5.3	1.5	3.0
40	8.3×10^4	2.2	1.8	3.6
60	7.3×10^4	1.3	1.6	3.2
80	6.3×10^4	0.88	1.5	3.0
100	5.5×10^4	0.63	1.4	2.8
150	3.9×10^4	0.28	1.2	2.4
200	2.8×10^4	0.12	1.0	2.02
250	2.0×10^4	0.054	0.86	1.7
300	1.4×10^4	0.024	0.74	1.5

[a] ρ = 8.3 g/mℓ.

[b] ρ = 1 g/mℓ.

The following equation[5] is used to calculate the Stokes diameter of an average agglomerate

$$d_s = \sqrt{\frac{-18V \frac{dC}{dt} \eta}{g\rho AC}} , \tag{2.6}$$

where

d_s = Stokes diameter (cm/sec),
V = volume of CRI-II vessel,
C = aerosol mass concentration (gm/mℓ),
t = time (sec),
η = viscosity of gaseous medium (= 2×10^{-4} P),
g = gravitational acceleration (= 980 cm/sec^2),
ρ = particle density (gm/mℓ),
A = floor area of the vessel (= 22,000 cm^2).

Substituting V/A = 209.4 cm into the equation above yields

$$d_s = \sqrt{\frac{-18\ (209.4)\ (2 \times 10^{-4})\ \frac{dC}{dt}}{980\ \rho\ C}} = \sqrt{\frac{-7.69 \times 10^{-4}}{\rho} \frac{dC/dt}{C}} . \tag{2.7}$$

Equation (2.4) can be written in the following form, in which time is in seconds:

$$C = 17\ e^{-0.00145t} + 3.15\ e^{-0.00027t} , \tag{2.8}$$

and

$$dC/dt = -0.00145(17)e^{-0.00145t} - 0.00027(3.15)e^{-0.00027t} . \tag{2.9}$$

Substituting Eqs. (2.8) and (2.9) into Eq. (2.7) yields

$$d_s = \sqrt{\frac{-7.69 \times 10^{-4}}{\rho} \left[\frac{-0.00145(17)\ e^{-0.00145t} - 0.00027(3.15)\ e^{-0.00027t}}{17\ e^{-0.00145t} + 3.15\ e^{-0.00027t}} \right]} . \tag{2.10}$$

Table 5. Calculated Stokes diameters of U_3O_8 aerosol particles from mass concentration measurements

Time (min)	Stokes diameters (μ)	
	$\rho = 8.3$	$\rho = 1$
5	3.3	9.5
10	3.23	9.3
15	3.1	8.9
20	2.94	8.5
40	2.27	6.5
60	1.81	5.2
80	1.6	4.6
100	1.6	4.6
150	1.6	4.6
200	1.6	4.6
250	1.6	4.6
300	1.6	4.6

Stokes diameters calculated from Eq. (2.10) for two density values are presented in Table 5.

2.3.3 Calculation of number of primary particles per average agglomerate

The determination of primary particle diameters of various fuel-oxide aerosols [either by the surface area (BET) method or by electron microscopy] gives an approach to calculate the number of particles per agglomerate for the branched-chained particles. An example is given in Table 6, where the calculation has been made for a typical run with each of the present aerosols. The number of primary particles per microgram of an agglomerate is simply

$$N\left(\frac{\pi}{6} D^3\right) \rho = 1 \times 10^{-6} . \qquad (2.11)$$

Using the BET surface areas and the equivalent average primary particle diameters at the material density of fuel oxides (10.9 for UO_2 and 8.3 for U_3O_8), values of >10,000 particles per agglomerate are calculated for

Table 6. Average number of primary particles per agglomerate for various aerosols

Aerosol type	Surface area (m^2/gm)	Average primary particle diameter (μm)	Time (min)	Primary particles per agglomerate
(UO_2)	13	0.044	20	6,600
CDV 16			200	15,600
(UO_2)	5.14	0.14	20	280
AF-10			200	610
(U_3O_8)	6.6	0.11	16	1,446
PT-20			80	3,065

the CDV aerosol, about 450 for the arc-furnace aerosol, and 2200 for the plasma torch aerosol. Photomicrographs and individual optical counting with a size comparator agree with these calculations. For the plasma torch aerosol, a typical photograph of agglomerates (Fig. 18) shows many particles with about the same average number of primary particles.

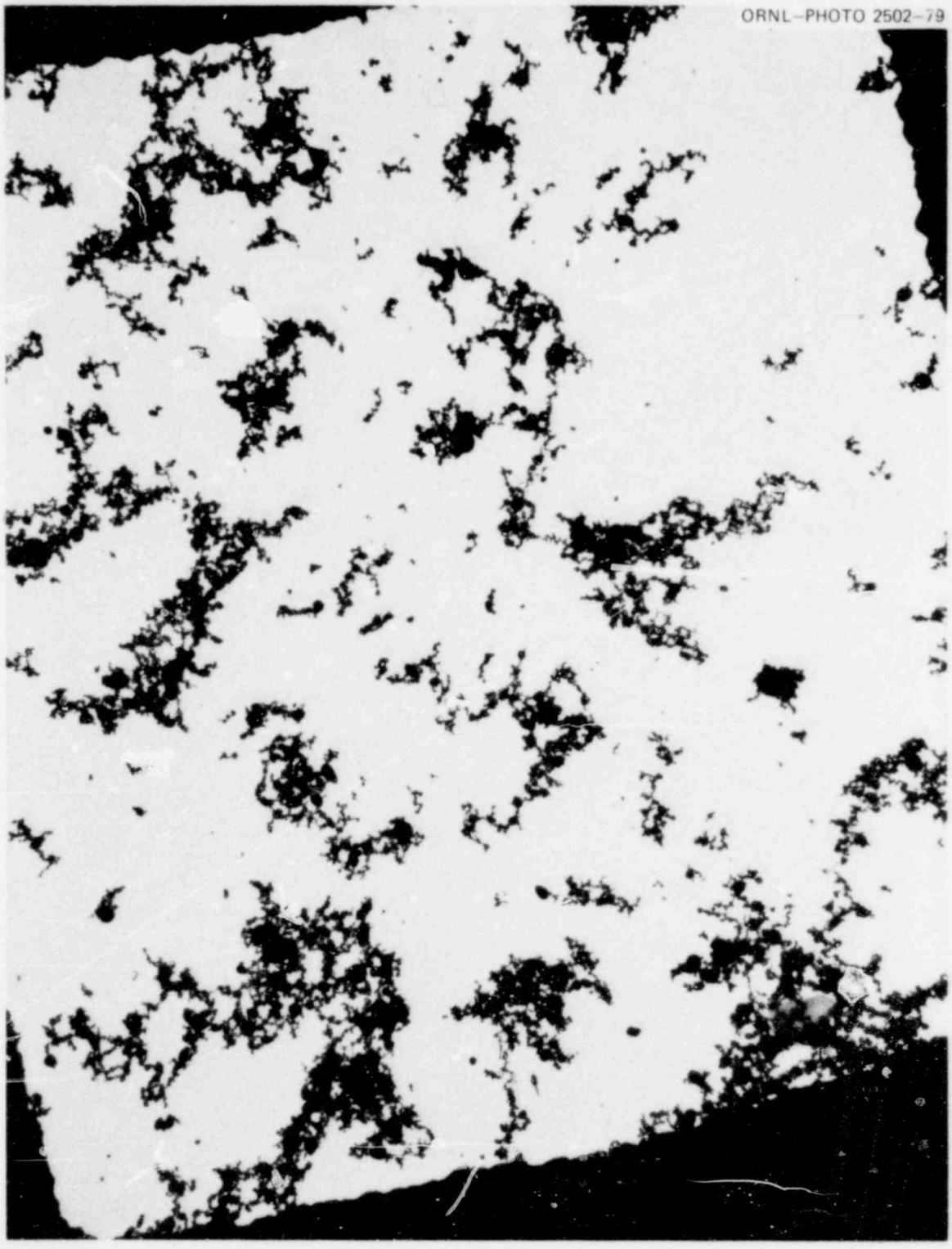

Fig. 18. Agglomerated U_3O_8 particles from run PT-17 initial fallout sample.

3. ANALYTICAL PROGRAM

J. T. Han

3.1 Evaluation of Fallout Model Using NSPP Data of Tests 106 and 107

The fallout model, which has been widely used in aerosol behavioral codes, including HAARM-3,[6] was utilized to estimate the fallout rates from the measurements of particle size distributions and aerosol mass concentrations obtained in the NSPP experiments. Comparisons of the calculated fallout rates with the experimental values were made to provide an evaluation of the fallout model. The present study presents the calculations obtained for the recent sodium spray fire experiments (tests 106 and 107)[1] along with previously obtained results for the sodium pool fire experiments (test 103 and 104).[3]

In the fallout model, the settling velocity of spherical particles, determined from Stokes' law neglecting buoyancy force,[3] is given as

$$V = \frac{d^2 \rho C g}{18 \mu_a} , \tag{3.1}$$

where

V = particle settling velocity (cm/sec),

d = particle diameter (cm),

ρ = particle density (g/cm^3),

C = Cunningham slip correction factor ($\simeq 1$ for NSPP sodium oxide aerosol),

g = acceleration of gravitation (cm/sec^2),

μ_a = air viscosity (g/cm-sec).

The fallout rate per unit floor area F is estimated by

$$F = Vm , \tag{3.2}$$

where m is the aerosol mass concentration (g/cm^3) measured in the experiment.

Figure 19 shows the aerodynamic diameter d_1 distributions measured with Andersen impactors in NSPP test 106 at two instances of time after

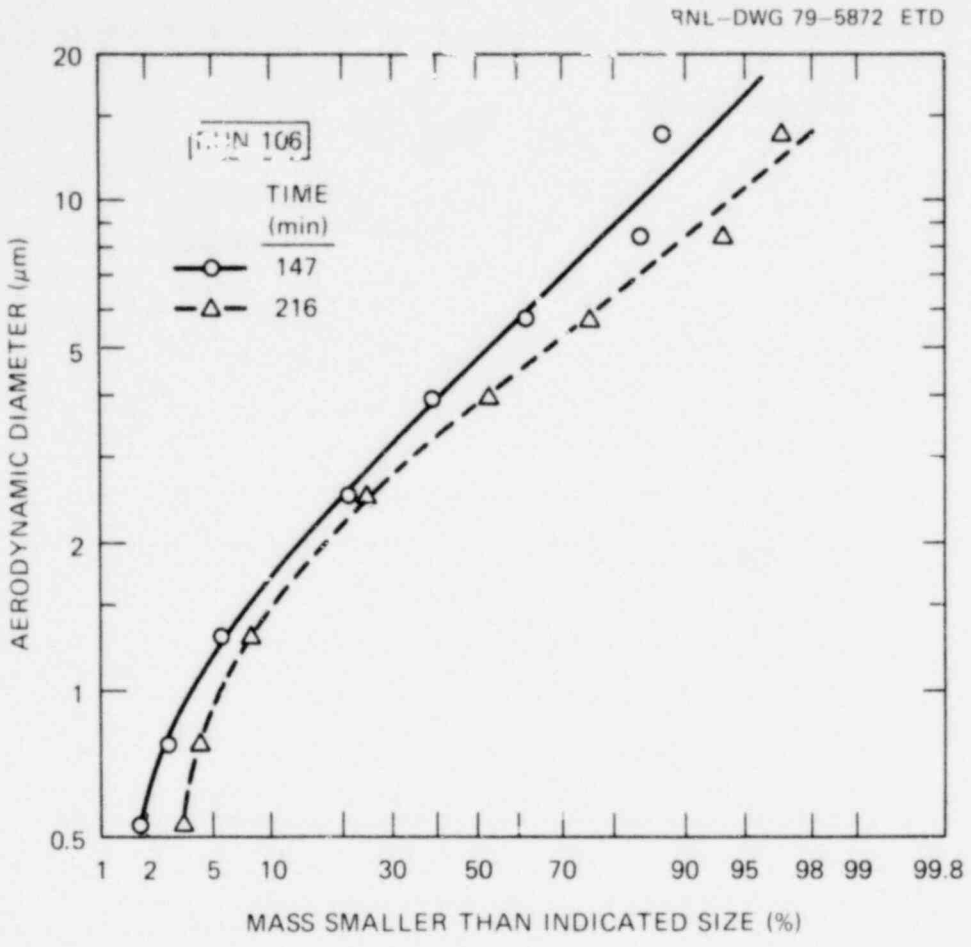

Fig. 19. Andersen stack impactor data for sodium oxide aerosol experiment of NSPP test 106.

the termination of aerosol generation. The actual particle diameter d can be estimated by $d = d_1/(\rho)^{1/2}$, assuming that the Cunningham slip correction factor is unity. Similarly, Fig. 20 shows the aerodynamic diameter distributions measured in NSPP test 107 at two instances of time after aerosol generation was completed. Calculations of average fallout velocities for tests 106 and 107 are presented, respectively, in Tables 7 and 8, where each settling velocity was determined by substituting the corresponding value of particle diameter d into Eq. (3.1) (using air properties at the corresponding measured temperature of 65 to 70°C).

Substituting the average fallout velocity for each case (from Tables 7 and 8, respectively) and the measured aerosol mass concentration into Eq. (3.2) yields the corresponding fallout rate per unit floor area.

Table 7. Particle diameter and estimated settling velocity of Na_2O aerosol in NSPP test 106

Range of mass (%)	Midpoint (%)	Aerodynamic diameter d (μm)[a]	Settling velocity V_i (cm/sec)	Average velocity $V = 0.20\ \Sigma V_i$ (cm/sec)
		At t = 147 min		
80–100	90	12.7	0.4327	0.667
60–80	70	7.15	0.1371	
40–60	50	4.79	0.0616	
20–40	30	3.18	0.0271	
0–20	10	1.74	0.0081	
		At t = 216 min		
80–100	90	8.61	0.1989	0.342
60–80	70	5.37	0.0774	
40–60	50	3.84	0.0396	
20–40	30	2.76	0.0204	
0–20	10	1.45	0.0056	

[a]Actual diameter = aerodynamic diameter/$(\rho)^{1/2}$.

Table 8. Particle diameter and estimated settling velocity of Na_2O aerosol in NSPP test 107

Range of mass (%)	Midpoint (%)	Aerodynamic diameter d (μm)[a]	Settling velocity V_i (cm/sec)	Average velocity $V = 0.20\ \Sigma V_i$ (cm/sec)
		At t = 145 min		
80–100	90	9.23	0.2265	0.351
60–80	70	5.50	0.0804	
40–60	50	3.59	0.0343	
20–40	30	1.88	0.0094	
0–20	10	<0.53	<0.0007	
		At t = 226 min		
80–100	90	7.29	0.1413	0.213
60–80	70	4.39	0.0512	
40–60	50	2.73	0.0198	
20–40	30	0.50	0.0007	
0–20	10	<0.50	<0.0007	

[a]Actual diameter = aerodynamic diameter/$(\rho)^{1/2}$.

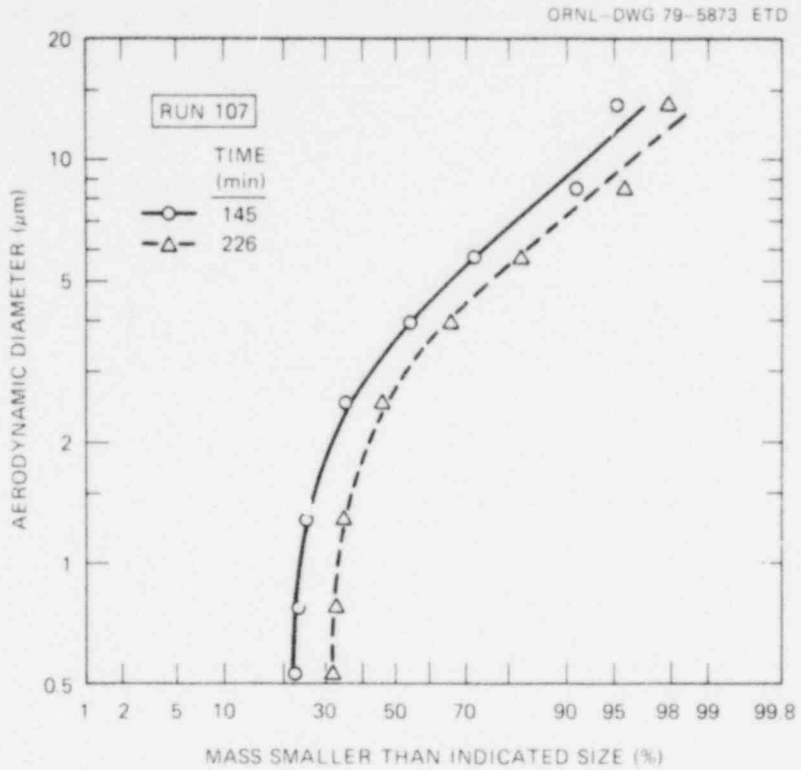

Fig. 20. Andersen stack impactor data for sodium oxide aerosol experiment of NSPP test 107.

Table 9. Comparison of fallout rates calculated by the model and NSPP data

Test	Time t (min)	Aerosol mass concentration ($\mu g/cm^3$)	Fallout rate per unit floor area ($\mu g/sec\text{-}cm^2$)		F_{model}/F_{exp}
			F_{model}	F_{exp}	
106	147	0.215	0.0287	0.0229	1.25
106	216	0.112	0.00766	0.0103	0.74
107	145	0.197	0.0138	0.0275	0.50
107	226	0.092	0.00392	0.0119	0.33

These results, along with the comparison with experimental data, are presented in Table 9. The fallout rates calculated by the model are of the same order of magnitude as the experimental data.

Figure 21 presents a summary of the comparison of the calculated and experimental fallout rates for tests 103, 104, 106, and 107. The agreement

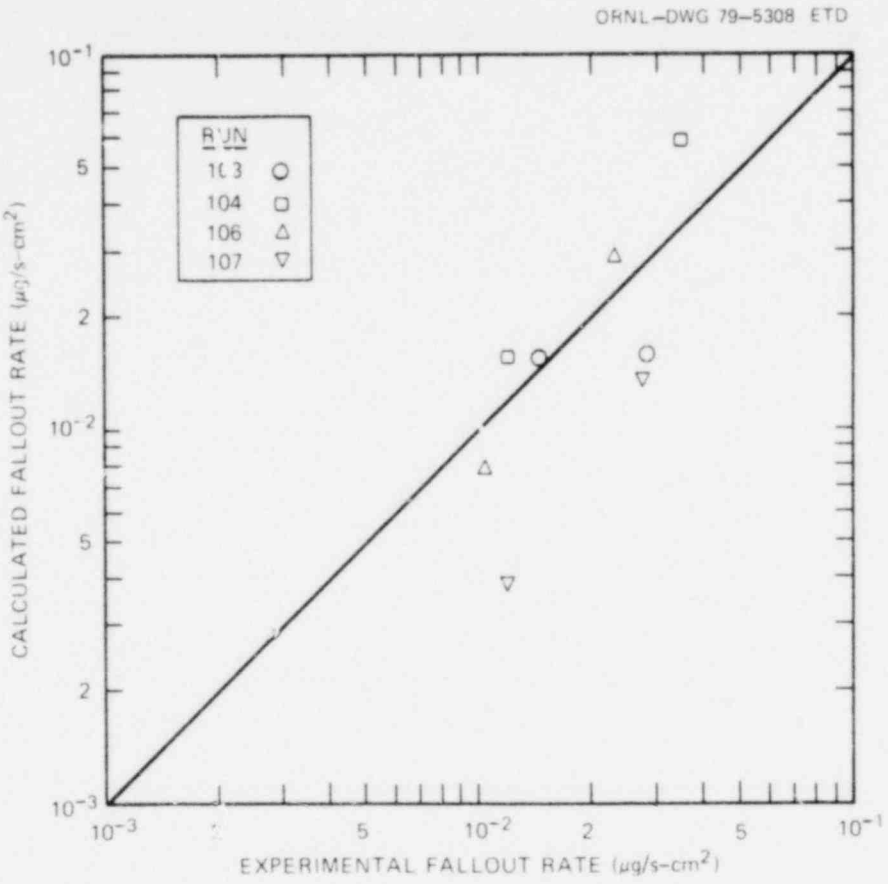

Fig. 21. Comparison of calculated and experimental fallout rates obtained in NSPP sodium oxide aerosol experiments of tests 103, 104, 106, and 107.

is reasonable, considering the uncertainty involved in the aerosol particle size measurements. Since the present fallout model is basically the same model as contained in the HAARM-3 code, this study provides some verification of the HAARM-3 fallout model.

3.2 Preliminary Calculation to Estimate Buoyancy-Induced Air Velocity in NSPP Vessel

Sodium oxide (Na_2O) aerosols have been generated in the Nuclear Safety Pilot Plant (NSPP) vessel[7] to simulate the aerosol release and transport in the LMFBR secondary containment during an HCDA. One of the objectives of the experiment is to provide data to validate the aerosol behavioral code, HAARM-3, in which the aerosol system is assumed to be

well-mixed. The purpose of the present study is to estimate the magnitude of the buoyancy-induced air velocity required to maintain a well-mixed aerosol system in the NSPP vessel.

Since the aerosol concentrations and temperature measurements at various locations in the vessel were approximately uniform, a practically well-mixed aerosol system did exist in the NSPP experiment. This was physically achieved by having a heated pan maintained at a constant temperature throughout the test (except in the first 10 to 20 min of the sodium fire, during which higher pan temperature occurred).

Figure 22 shows the location of the heated pan in the NSPP vessel. The vessel has a volume of 38.3 m^3, an average height of ~5.24 m (= vessel volume/cross-sectional area of the vessel), and a diameter of 3.05 m. The heated surface is located about 1 m above the center of the vessel floor and is maintained at a constant temperature T_h. It is assumed that the vessel wall is maintained at a constant temperature T_c, and the bulk air temperature is at T_∞.

Theoretically, the value of T_∞ can be estimated from the values of T_h and T_c. Assuming quasi-steady-state heat transfer in the vessel,

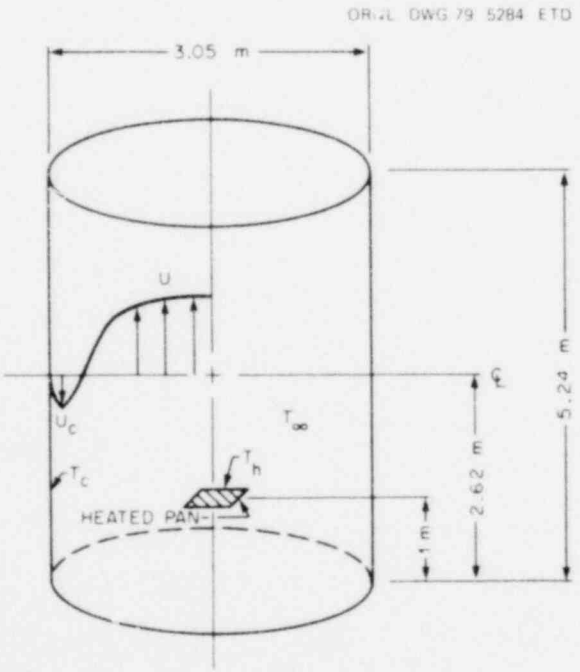

Fig. 22. Simplified representation of NSPP vessel with heated pan.

the following equation is obtained:

$$h_p A_p (T_h - T_\infty) = [h_1 A_1 + (h_2 + h_3) A_2](T_\infty - T_c) \ , \qquad (3.3)$$

where

h_p = natural-convection heat transfer coefficient at the heated pan,

A_p = surface area of the heated pan = 0.805 m^2 (= 4.33 × 2 ft^2),

A_1 = area of the internal vertical surface = 50.2 m^2 (540.5 ft^2),

A_2 = area of the vessel ceiling or floor = 7.31 m^2 (78.7 ft^2),

h_1 = heat transfer coefficient at the vessel internal vertical surface,

h_2 = heat transfer coefficient at the vessel ceiling,

h_3 = heat transfer coefficient at the vessel floor.

In the equation above, the heat transfer coefficients are dependent on the value of T_∞; the trial-and-error iterative technique has to be used to calculate T_∞. The values of T_∞ calculated from Eq. (3.3), in comparison with those measured in NSPP tests 103 and 104, are given in Table 10. The calculated values fall within the range of the data measured by 20 thermocouples at various locations inside the vessel. The average heat transfer coefficient at each surface is calculated from the empirical formulas given in Holman.[8]

To estimate the plume rise velocity U at the horizontal midplane of the vessel (Fig. 22), the solution presented by Morton et al.,[9,10] is used, assuming a point heat source and uniform velocity profiles in the plume. Thus,

$$U = 3.73\, Q^{1/3} x^{-1/3} \ , \qquad (3.4)$$

$$R = 0.12x \ , \qquad (3.5)$$

and

$$Q = R^2 U g(\rho_\infty - \rho)/\rho_\infty \ , \qquad (3.6)$$

Table 10. Comparison of the calculated T_∞ and the experimental values for two NSPP tests at $50 \leq t \leq 67$ min

	NSPP test	
	103	104
T_h, °C	250	250
T_c, °C[a]	49	68
T_∞, °C[b]	59–60	68–90
H_p, W/m²-°C	7.34	7.02
H_1, W/m²-°C	2.67	2.55
H_2, W/m²-°C	2.88	2.75
H_3, W/m²-°C	0.805	0.784
$T_{\infty,cal}$, °C	56	74

[a] Average of two thermocouple readings.

[b] Measured by 20 thermocouples at various locations inside the NSPP vessel.

where

x = vertical distance between the plume and the virtual point source (located below the heated pan),

R = radius of the plume at location x,

Q = buoyancy flux of the plume = a constant.

To determine the location of the virtual point heat source, the rectangular heated pan is replaced by a disk at the same surface temperature T_h and with the same surface area. For the conditions presented in Table 10, the fictitious disk will release approximately the same amount of heat into the ambient vessel air as the heated pan. The radius of the fictitious disk is found to be 0.506 m, and the corresponding value of x from Eq. (3.5) is 4.22 m. Therefore, the distance between the horizontal midplane of the vessel and the virtual point heat source of the plume is

5.84 m (= 4.22 m + 1.62 m). The air density at the horizontal midplane of the vessel can be calculated from the temperature measurements in the NSPP experiment. Substituting the values of density ρ and the vertical distance x of 5.84 m into Eqs. (3.4) through (3.6), the plume velocity U at the vessel horizontal midplane is obtained. The results are presented in Table 11 for NSPP tests 103 and 104. The maximum downward velocity U_c at the vessel horizontal midplane (Fig. 22) is also presented in Table 11. Since the buoyancy-induced boundary layer flow along the cold vertical wall was turbulent (at $Gr_x > 4 \times 10^8$), Cheesewright's data[11] were used: $U_c \simeq 0.29\ [gx(T_\infty - T_c)/T_\infty]^{0.5}$, with x = 2.62 m. Should the boundary layer flow have been laminar, Ostrach's analytical result[12] would yield $U_c = 0.56\ Gr_x^{0.5}\ \nu/x$, which is also presented in Table 11.

Table 11. Estimated plume velocity U and maximum downward velocity U_c at horizontal midplane of the NSPP vessel at $50 \leq t \leq 67$ min

	NSPP test	
	103	104
U, m/s (ft/sec)	0.36 (1.2)	1.0 (3.3)
U_c, m/s (ft/sec)	0.21 (0.69)	0.19 (0.62)
U_c, m/s (ft/sec)[a]	0.40 (1.3)	0.38 (1.2)

[a] Based on laminar boundary layer calculation.

In summary, the buoyancy-induced air velocity has been estimated for NSPP tests 103 and 104 using a simple analytical method. A practically well-mixed aerosol system was found to exist in the NSPP vessel when the midplane plume velocity was at an estimated value of 0.36 m/sec (1.2 ft/sec) or larger.

3.3 Drag Coefficient of Spherical Aerosol Particles

In the HAARM-3 aerosol code,[6,13] the drag coefficient of spherical aerosol particles is calculated with one of the following formulas[14,15] as

specified by the user: (1) Stokes' law of $C_D = 24/Re$, and (2) Klyachko's correlation of $C_D = 24/Re + 4/Re^{1/3}$. Stokes' law is applicable only for Reynolds number values less than unity, whereas Klyachko's correlation has been recommended for Reynolds number values in the range of $3 \leq Re \leq 400$. For aerosol systems containing a wide spectrum of particle sizes, the drag coefficient may not be accurately calculated by use of either formula alone. Therefore, the HAARM-3 code could be improved by the incorporation of a built-in capability to choose the appropriate formula for the drag coefficient calculation based on the Reynolds number of the particle. The following correlation is recommended:

$$C_D = \frac{24}{Re} + \frac{4}{Re^{1/3}} f(Re) \ , \tag{3.7}$$

where

C_D = drag coefficient = $D/(\pi d^2 \rho_a V^2/8)$,
D = the drag of the particle,
d = particle diameter,
ρ_a = density of the ambient air,
V = relative velocity between the particle and the air,
Re = Reynolds number of the particle = $\rho_a V d/\mu_a$,
μ_a = air viscosity,
$f(Re)$ = a function of the Reynolds number,
$f(Re) = 0$ at $Re < 0.3$,
$f(Re) = 1$ at $0.3 \leq Re \leq 650$.

Table 12 shows the excellent agreement between the drag coefficients calculated with Eq. (3.7) and the experimental measurements,[14] with a deviation of <5% at $Re \leq 650$. The recommended correlation is, therefore, applicable for most aerosol systems in which the particle Reynolds numbers seldom exceed 100.

Table 12. A comparison of the calculated drag coefficients and the experimental measurements for spherical particles in air

Re	$C_{D,cal}$[a]	$C_{D,exp}$	$C_{D,cal}/C_{D,exp}$
0.05	480	483.1	.994
0.1	240	243.8	984
0.2	120	123.6	0.971
0.25	96.0	99.32	0.967
0.3	95.98	83.21	1.03
0.5	53.04	50.90	1.04
1	28.0	26.92	1.04
3	10.77	10.58	1.02
10	4.257	4.325	0.984
100	1.102	1.094	1.01
200	0.8040	0.7980	1.01
400	0.6029	0.6114	0.986
500	0.5520	0.5680	0.972
600	0.5143	0.5368	0.958
650	0.4987	0.5241	0.952

[a] $C_{D,cal} = 24/Re + 4f(Re)/Re^{1/3}$, where $f(Re) = 0$ at $Re < 0.3$ and $f(Re) = 1$ at $0.3 \leq Re \leq 650$.

REFERENCES

1. T. S. Kress and M. L. Tobias, *LMFBR Aerosol Release and Transport Program Quart. Prog. Rep. October–December 1978* (to be published).
2. A. L. Wright, A. M. Smith, and T. S. Kress, *Fuel Aerosol Simulant Test (FAST) Plan*, ORNL/NUREG/TM-129 (September 1977).
3. T. S. Kress and A. L. Wright, *LMFBR Aerosol Release and Transport Program Quart. Prog. Rep. July–September 1978*, ORNL/NUREG/TM-276 (January 1979).
4. O. G. Raabe et al., "Aerodynamic and Dissolution Behavior of Fume Aerosols Produced During Combustion of Laser-Ignited Plutonium Droplets in Air," *Health Phys.* 35, 663–74 (November 1977).
5. R. K. Hilliard et al., "Sodium Oxide/Hydroxide Aerosol Properties and Behavior in a Large Vessel," *Fifteenth DOE Nuclear Air Cleaning Conference, August 7–10, 1978*, CONF-780819 (February 1979).
6. J. A. Gieseke, K. W. Kee, and L. D. Reed, *HAARM-3 Users Manual*, BMI/NUREG-1991 (January 1978).
7. R. E. Adams, T. S. Kress, and L. F. Parsly, Jr., *Sodium-Oxide Aerosol Study: NSPP Runs 101–105, Data Record Report*, ORNL/NUREG/TM-179 (April 1978).
8. J. P. Holman, *Heat Transfer*, 2nd ed., pp. 197–99, McGraw-Hill, New York, 1968.
9. B. R. Morton, G. Taylor, and J. S. Turner, "Turbulent Gravitational Convection from Maintained and Instantaneous Sources," *Proc. Roy. Soc. London, Ser. A* 234, 1–23 (1956).
10. J. S. Turner, "Buoyant Plumes and Thermals," *Annu. Rev. Fluid Mech.* 1, 29–44 (1969).
11. R. Cheesewright, "Turbulent Natural Convection from a Vertical Plane Surface," *J. of Heat Transfer*, 1-8 (February 1968).
12. E. R. G. Eckert and R. M. Drake, Jr., *Analysis of Heat and Mass Transfer*, p. 529, McGraw-Hill, New York, 1972.
13. K. K. Lee, private communication, March 30, 1979.
14. N. A. Fuchs, *The Mechanics of Aerosols*, pp. 30–33, Pergamon Press, Oxford, England, 1964.
15. R. Dennis, *Handbook on Aerosols*, TID-26608, pp. 45–46 (1976).

NUREG/CR-0844
ORNL/NUREG/TM-329
Dist. Category R7

Internal Distribution

1. R. E. Adams
2. M. Bender
3. H. W. Bertini
4. J. R. Buchanan
5. W. B. Cottrell
6. G. F. Flanagan
7-8. M. H. Fontana
9-11. J. T. Han
12. H. W. Hoffman
13-17. T. S. Kress
18. Milton Levenson
19. R. E. MacPherson
20. F. R. Mynatt
21. G. W. Parker
22. L. F. Parsly
23. P. Patriarca
24. J. L. Rich
25. J. M. Rochelle
26. A. M. Smith
27. I. Spiewak
28. A. L. Sutton, Jr.
29. D. G. Thomas
30. M. L. Tobias
31. H. E. Trammell
32. D. B. Trauger
33. J. L. Wantland
34. J. S. White
35. G. D. Whitman
36. A. L. Wright
37-38. Central Research Library
39. Y-12 Document Reference Section
40-42. Laboratory Records Department
43. Laboratory Records (RC)

External Distribution

44. J. T. Larkins, Experimental Fast Reactor Safety Research Branch, Division of Reactor Safety Research, Nuclear Regulatory Commission, Washington, D.C. 20555
45-48. Director, Office of Nuclear Regulatory Research, Nuclear Regulatory Commission, Washington, D.C. 20555
49. Office of Assistant Manager, Energy Research and Development, DOE, ORO
50-51. Technical Information Center, DOE
52-361. Given distribution as shown in category R7 (NTIS-10)

☆U.S. GOVERNMENT PRINTING OFFICE: 1979-640-079/137